MODELING AND ANALYSIS OF DUAL HYDROFORMING PROCESS

A Thesis

by

NISHANT JAIN

Submitted to the Office of Graduate Studies of
Texas A&M University
in partial fulfillment of the requirements for the degree of

MASTER OF SCIENCE

December 2003

Major Subject: Mechanical Engineering

MODELING AND ANALYSIS OF DUAL HYDROFORMING PROCESS

A Thesis

by

NISHANT JAIN

Submitted to Texas A&M University
in partial fulfillment of the requirements
for the degree of

MASTER OF SCIENCE

Approved as to style and content by:

_____
Jyhwen Wang
(Co-Chair of Committee)

_____
Richard Alexander
(Co-Chair of Committee)

_____
Karl Hartwig
(Member)

_____
Dennis L. O'Neal
(Head of Department)

December 2003

Major Subject: Mechanical Engineering

ABSTRACT

Modeling and Analysis of Dual Hydroforming Process.

(December 2003)

Nishant Jain, B.E., Bangalore University, India

Co-Chairs of Advisory Committee: Dr. Jyhwen Wang
Dr. Richard Alexander

The tube hydroforming process has gained increasing attention in recent years. Coordination of the internal pressurization and axial feeding curves is critical in the tube hydroforming process to generate successful parts without fracture or wrinkling failure. The stress state at a given time and location varies with the process history and the design and control of the load paths. A new process parameter, counter-pressure, is introduced to achieve a favorable tri-axial stress state during the deformation process. The new process is referred to as *dual hydroforming*.

The benefits offered by dual hydroforming will be characterized based upon the amount of wall thinning, plastic instability limit and final bulged configuration. An analytical model is developed to analyze the stress and strain state in the part (tube) during the dual hydroforming process. The stress-strain condition analyzed will be used to evaluate and compare thinning for tube hydroforming and dual hydroforming. The effect of applying counter-pressure on the plastic instability of thin-walled tubes with only internal pressure and combination of internal pressure and independent axial loading is considered. Finite

element analysis is used to quantify the merits of dual hydroforming in terms of final bulged configuration. A parametric study has been conducted to investigate the effectiveness of dual hydroforming based on the various material properties and process conditions.

Dual hydroforming results in different stress and strain states compared to tube hydroforming. The counter-pressure enabled favorable tri-axial stress state during deformation that resulted in different thickness and percentage thinning. Finite element analysis showed that for a particular amount of wall thinning there is an increase of around 8% in bulge height for dual hydroforming. Dual hydroforming delays the onset of plastic instability. This increase in the value of effective strain to failure results in an increase of around 12% in bulge height for dual hydroforming as shown by finite element simulations.

Results of this study indicate that dual hydroforming can increase expansion i.e. more difficult parts can be designed and manufactured. Also, for a given part geometry, higher strength and less formable materials can be used.

ACKNOWLEDGEMENTS

It has been well said by Shakespeare that *"Pupil Thy Work Is Incomplete, Till Thee Thank the Lord and the Masters"* and I sincerely believe this.

It is a pleasure to thank the many people who made this research possible. It is difficult to overstate my gratitude to my advisor, Dr. Jyhwen Wang. He provided me this opportunity to work in this inspiring project. With his enthusiasm, inspiration, and great efforts to explain things clearly and simply, he helped to make this investigation fun. Throughout my research-writing period, he provided encouragement, sound advice, good teaching, good company, and lots of good ideas. I would have been lost without him. I have learned many things from him such as the way of thinking and the way of conducting research.

It gives me immense pleasure in expressing my heartfelt gratitude to Dr. Richard Alexander for all the cooperation he has rendered in the successful completion of this work. I am most appreciative of the instructions I received during my discussions with him. I am sure that these invaluable lessons about presentation skills will provide me with a strong foundation for my future work. I am profusely grateful to Dr. Karl Hartwig for serving on my thesis committee and being ever ready to go through any formalities.

I would like to thank my family and friends who have been very helpful in this endeavor.

My parents have always encouraged me and guided me to independence, never trying to limit my aspirations. I would like to express my sincere gratitude to my brother who has always been encouraging.

I also wish to acknowledge the services of all those who have helped me directly or indirectly from the Texas A&M University System in carrying out this project.

TABLE OF CONTENTS

LIST OF FIGURES

LIST OF TABLES

NOMENCLATURE

σ_1, σ_2 and σ_3	Principal stresses
ε_1, ε_2 and ε_3	Principal strains
$d\varepsilon_1$, $d\varepsilon_2$ and $d\varepsilon_3$	Incremental principal strains
σ_θ	Hoop stress
σ_z	Longitudinal stress
σ_r	Radial stress
σ_{ra} and σ_{ra}	Radial stress at inner and outer radius
σ_{za} and σ_{zb}	Axial stress at inner and outer radius
ε_θ	Hoop strain
ε_z	Longitudinal strain
ε_t	Radial strain
$\bar{\sigma}$	Effective stress
$\bar{\varepsilon}$	Effective strain
L	Original length (uniaxial test)
r	Mean radius of tube
t_o	Initial thickness of tube
t_i	Instantaneous thickness of tube
p_i	Internal pressure
p_o	Counter pressure

K	Strength co-efficient
n	Strain hardening parameter
z	Sub-tangent modulus

CHAPTER I

INTRODUCTION

Tube hydroforming has been well-known since the 1950's. Tube hydroforming has been called by many other names such as bulge forming of tubes (BFT's), liquid bulge forming (LBF) and hydraulic (or hydrostatic) pressure forming (HPF) depending on the time and country in which it was used [1]. Tube hydroforming (THF) has become a viable method for manufacturing complex automobile parts and an indispensable manufacturing technique in recent years. Hydroformed tube parts have improved strength and stiffness, lower tooling cost, fewer secondary operations, and closed dimensional tolerances compared to stamping processes, thus an overall reduced manufacturing cost [1]. Success of the tube hydroforming process depends on an appropriate combination of loading curve (internal pressure and axial feed at the tube ends), material properties and process conditions. One of the key concerns is to control the deformation process in order to maximize the expansion so that more complex shapes in various applications can be achieved. Analogously, for a given shape a higher strength, lighter weight, less formable, or lower cost material can be adopted.

The thesis follows the style and format of ASME Journal of Manufacturing Science and Engineering.

The process cycle for a typical tube hydroforming operation follows the sequence illustrated in Fig. 1-1.

1. The tube is placed between the dies.

2. Clamping device is used to close the dies and to apply sufficient clamping force.

3. Tube is filled with hydraulic fluid to provide necessary internal pressure.

4. Axial punches are used to provide initial sealing to avoid any pressure losses.

5. Fluid pressure within the tube is increased after the die closes to cause necessary deformation with simultaneous application of axial feeding to push the material into the deformation zone. The proper combination of axial feeding and internal pressure are applied during the hydroforming process to improve hydroforming capabilities. Once the tube touches the die, the calibration phase starts. Axial feeding is not required during the calibration phase. Tube is subjected to large pressures to form corner radii.

6. Finally, the bulged tube is taken out of the die.
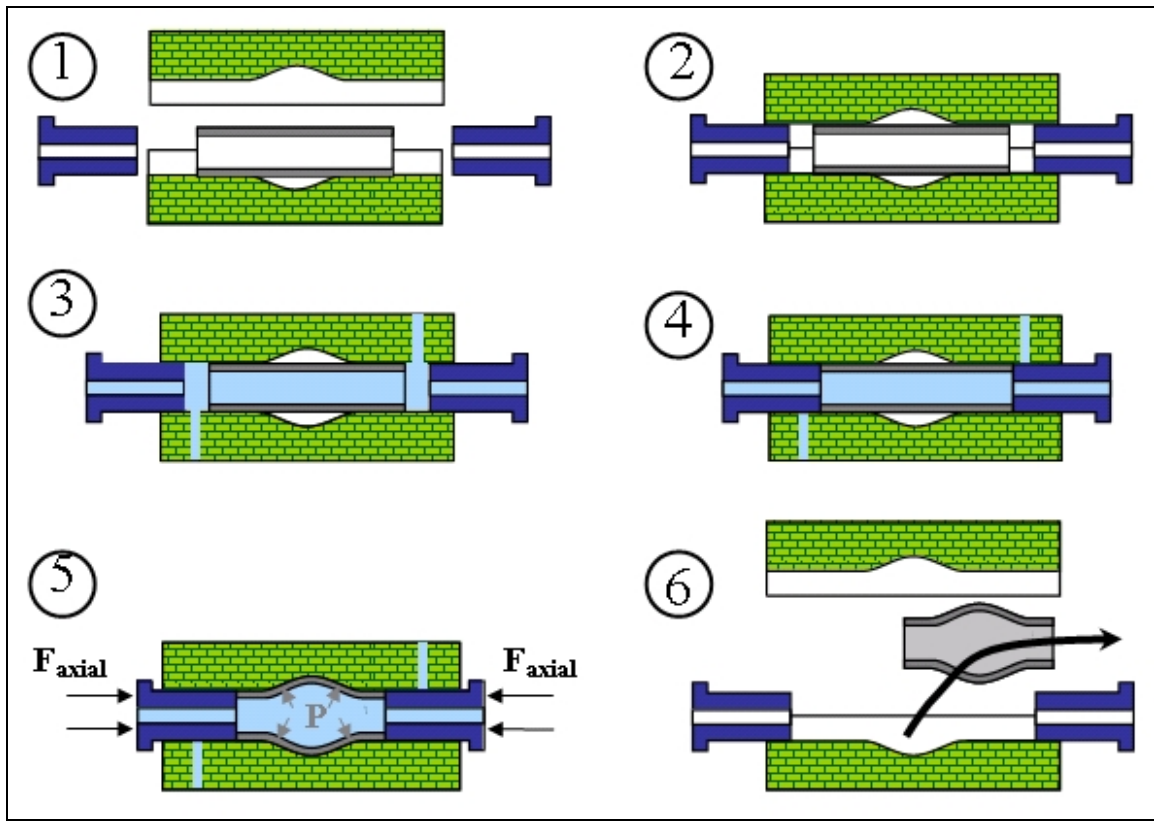
Figure 1-1: Process Sequence- Tube Hydroforming (Adapted from: Siempelkamp
Pressen Systeme GmbH & Co)

1.1 Research Objective

As explained above, tube deformation is controlled by 'gradually' increasing the internal
pressure during the application of axial load (Fig. 1-2). In reality, the final bulged
configuration obtained from the forming process deviates depending on the load paths.
Thus, process design and control play a key role in the success or failure of the tube
hydroforming operation. The objective of the proposed research is to extend the
boundary of current tube hydroforming process capability through the application of

counter pressure. The process will be referred to as dual hydroforming (Fig. 1-2). In dual hydroforming, control deformation (avoiding bursting or fracture, wrinkling and buckling) will be achieved with a proper combination of internal pressure, axial feed and counter pressure.
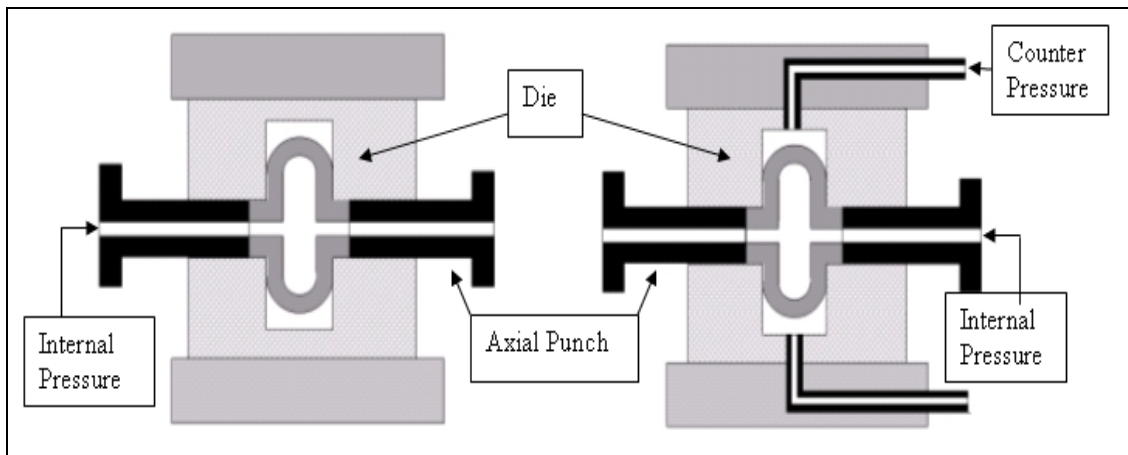
Figure 1-2: Tube Hydroforming and Dual Hydroforming

The counter-pressure will provide back support to the tube material and hence will result in less thinning and a delayed onset of plastic instability. Inversely, larger tube expansion can be achieved. Also, for a given part geometry, higher strength and less formable materials can be used.

1.2 Research Plan

The benefits offered by dual hydroforming will be characterized based upon their effect on the amount of thinning, plastic instability (fracture) and final bulged configuration. The present work is broadly divided into three main categories listed below.

1. The stress state at a given time and location varies with the process history and the design and control of the load paths. Since the loading condition in dual hydroforming is different from that of the tube hydroforming, an analytical model is developed to analyze the stress and strain state in the part during the dual hydroforming process. The stress strain condition analyzed will be used to evaluate and compare thinning for tube hydroforming and dual hydroforming processes. The effect of applying counter pressure is also evaluated using finite element simulations based on the final configuration achieved.

2. Successful tube hydroforming requires the bulging to take place without causing any type of instability like bursting, necking, wrinkling or buckling. Excessive pressure without sufficient axial feed will cause the tube to fracture while excessive application of axial force will lead to wrinkling of the tube. The effect of applying counter-pressure on the plastic instability of thin-walled tubes with only internal pressure and a combination of internal pressure and independent axial loading is considered. The instability criterion will yield effective strain to failure for dual hydroforming process. The effect of plastic instability on the final bulged configuration for dual hydroforming is depicted through finite element simulations.

3. The tube material properties, such as yield strength, anisotropic values, hardening exponent and process conditions such as friction, affect the tube deformation process. A parametric study is conducted using finite element simulations to investigate the effects of material parameters and friction on the dual hydroforming process.

1.3 Literature Survey

The hydrostatic stresses have been successfully used in many manufacturing techniques such as sheet hydroforming, deep drawing, wire drawing and extrusion etc. During deformation, limiting strains (fracture strains) depend upon the level of hydrostatic stress [2]. High hydrostatic pressure suppresses void growth, thereby delaying fracture [3]. There is a loss of density by growth of micro porosity during strip drawing, and Rogersand et al. studied the effect of superimposed hydrostatic pressure on diminishing the density loss [4]. The results showed that drawing at the highest pressure level increased the density, presumably by closing preexisting pores formed during earlier processing. The formability problems could be minimized if all stress components could be maintained compressive. Materials of very limited formability can be successfully extruded if both the billet and die exit region are under high hydrostatic pressure [2]. Hosford and Caddell [2] showed that mean stress and the largest principal stress usually increase or decrease together. Cockcroft and Latham [5] have suggested a fracture criterion that associates the dependence of fracture strain upon hydrostatic stress. They

performed tensile tests under superimposed hydrostatic pressure for various materials. They reported that for some cases appreciably larger strains were observed from final separation. Other fracture criteria have also been proposed [6, 7, 8] identifying the reliance of limit strain upon hydrostatic stress.

The motivation to apply the counter pressure in the tube hydroforming process comes from the fact that counter pressure has been used effectively in many manufacturing processes to enhance the manufacturing capabilities. The most notable work related to the counter pressure approach is in *sheet hydroforming* research (Finckenstein [9], Thiruvarudchel [10], Altan [11], Hein [12]). It was suggested that counter pressure could suppress wrinkling and prevent fracture. Liu et al. [13] evaluated sheet metal formability using a viscous pressure forming dome test. Based on the proposed critical damage value criterion and the experimental results, it was found that the formability of the sheet stretched with viscous pressure was higher than that obtained with a solid hemispherical punch. In their paper, the feasibility of applying counter pressure was discussed but not implemented. Lo et. al. [14] used the upper bound-lower bound approach to develop load paths for hemispherical stretch forming. The punch deforms the work piece by forcing it against a controlled pressurized fluid. It can be observed that deformation geometry of the hemispherical stretch forming is comparable to that of the pole on the free bulging of tubes. Analytical models were developed by Yossifon [15, 16] to predict the results in deep drawing. It was shown that a pressure load path lying between the derived upper (causes fracture) and lower (causes wrinkling) limits can be identified and

recommended for practical use. Ahmed and Hashmi [17] simulated bulge forming of a circular plate by applying a restrained load on three central elements at the top surface. The restrained forming resulted in better configuration than the conventional bulge forming. The papers presented by Nakagawa [18] and Amino [19] summarize the various merits and applications of hydraulic counter-pressure deep drawing. Industrial applications of the process were also demonstrated.

Successful tube hydroforming requires the bulging to take place without causing any type of instability like bursting, necking, wrinkling or buckling. Excessive pressure without sufficient axial feed will cause the tube to fracture while excessive application of axial force will lead to wrinkling of the tube. Thus, as shown in Fig. 1-3, the *counter force* has been used on significant regions in T-shape and Y-shape protrusions that allow the internal pressure to be increased beyond the critical value [20]. It was reported by Tonghai [21] that use of counter force in the elastomer forming process increased the obtainable protrusion height to 1.5 times of the original diameter for low carbon steel tubes whereas the expansion ratio without counter force was found to be 1.2. Koc et. al. [20] presented various applications of counter force.

The crucial goal in THF is to obtain a better part without causing any type of instability. The point of fracture failure can be prevented by controlling the deformation rather than providing the axial force that may cause wrinkling. As explained earlier, in some cases like axisymmetric bulging, counter force cannot be applied due to inherent constraint.

The part geometry precludes the case of counter punch. It is not possible to design a counter punch tool for a simple axis-symmetrical bulge forming process. Also, the effect of the counter punch is not on the whole part of bulge and instead is concentrated on a localized area. Thus, the application of a dual pressure system as shown in Fig. 1-3 to increase the bulge height is a logical alternative.
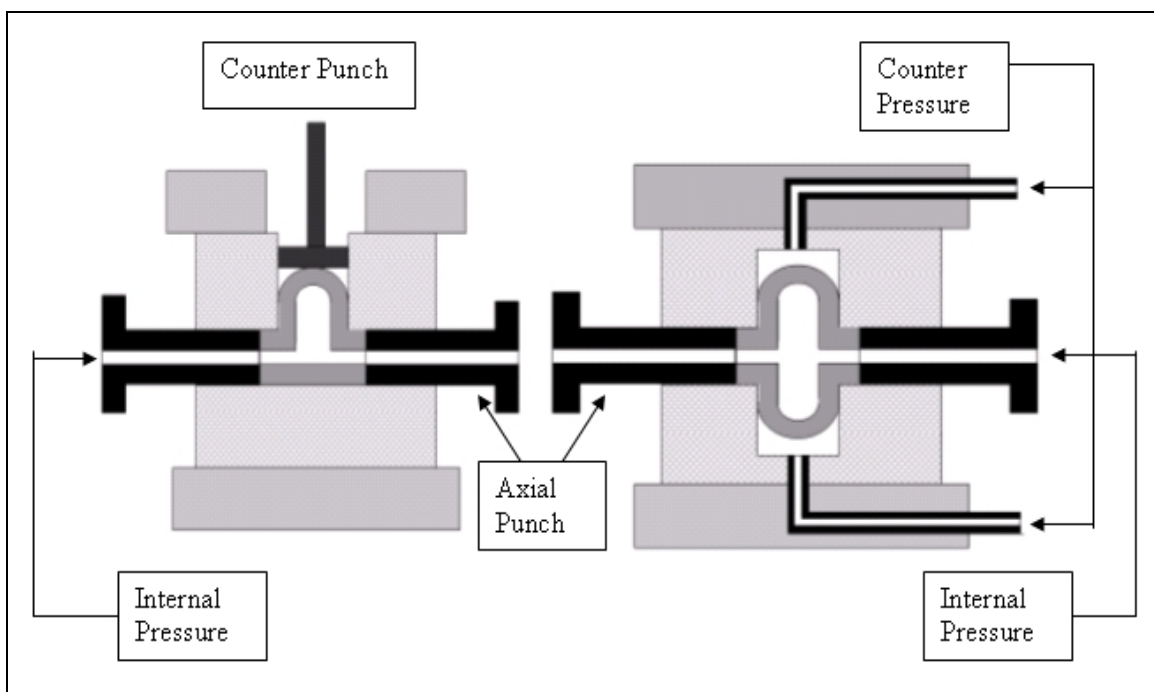
Figure1-3: Counter Punch and Dual Hydroforming

Over the years, plastic instability has been studied in detail for different manufacturing processes, including tube hydroforming. In his early work, Mellor presented an analytical solution giving the conditions at instability of a thin-walled tube subjected to internal pressure and independent axial load [22]. Hiller presented tensile plastic

instability under complex stress [23]. He deduced the criterion of instability from work principle and applied the same to the thin tubes under internal pressure and an independent axial load. He emphasized that there may be more than one solution to a given problem depending on how the load rates are specified. For the thin-walled tube he considered three cases of loading, in which, the case of proportional stressing resulted in the same instability criterion as presented by Mellor. Hiller presented a critical study of apparently conflicting theories of the instability of tubes subject to internal pressure and an independent axial load [24]. He showed that each theory is in fact a solution of the problem subjected to different type of constraints on the loading path. Hiller presented the effect of pressure on the ductility of metal subjected to some sheet forming processes such as process with bi-axial stress, expansion of spherical shell and bulging of circular diaphragm [25]. In all the cases he considered, the ductility was found to be increased by the presence of fluid pressure on the sheet surface. Chakrabarty et al. presented a method to accurately determine the instability strain for thick walled cylinders using a closed form expression of the pressure-expansion relationship [26]. El-Sebaie et al. calculated plastic instability conditions for deep drawing in a high pressure medium [27]. They showed that the limiting drawing ratio was increased from 2.19 to 3.44 for the pressure process.

Various parametric studies have been done to analyze the effect of material properties on tube hydroforming. Carleer et al. stated that in order to achieve the most economic product with the best performance, it is important to choose proper material and process

parameters [28]. The experiments were conducted on various steel grades ranging from high strength to low strength steels. The material parameters studied were the hardening exponent (*n*) and the plastic anisotropic parameter (*r*). They highlighted the anisotropy value and friction parameter having the largest effect on strain distribution. Manabe et al. explored the effects of process parameters, material properties and die shape on the deformation process in die-bulge forming. Earlier investigations have been on free bulge forming [29]. They used the nonlinear explicit FEM commercial code LS-DYNA3D to carry out a parametric study for different anisotropic values, strain hardening parameters, stress ratios and coefficients of friction. It was concluded that plastic anisotropy is one of the most important material parameters for the tube hydroforming. Boudeau et al. developed a numerical approach that permits the prediction of necking from finite element results [30]. Material properties of steel and aluminum alloy were used to highlight the influence of materials and process parameters. Koc considered the effect of material properties as a crucial aspect of tube hydroforming technology. He investigated the effects of loading path and material property variations on part quality specifications and production equipment capacity requirements [31]. The experiments were conducted to characterize the influence of the strain hardening exponent and anisotropy on forming of tubes.

The load curve (variation of internal pressure, axial load and counter pressure with time) defines the load history and is influenced by material, shell thickness, tube diameter, the relationship between shell thickness and the tube diameter, and the forming radius [32 -

34]. Many researchers have presented theoretical and practical work on the estimation of load parameters for tube hydroforming using various techniques [35 - 37]. Asnafi et al. studied the stroke controlled free forming, theoretically and experimentally [35]. He derived the pressure and magnitude of stroke at yield limit as well as during plastic deformation. Rimkus et al. describe the principles involved in the design of load-curves for the simulation [36]. They suggested that to conduct a simulation of the forming process accurately using the finite element method (FEM), it is necessary to calculate the axial force necessary to control the course of the wall thickness, the forming pressure necessary to press the tube into the tool, and the calibration pressure necessary to form the (smaller) radii. Koc et al. presented analytical models to predict buckling, wrinkling and bursting as well as to calculate axial force, internal pressure and counter force in tube hydroforming based of force balance analysis [20].

CHAPTER II

TUBE HYDROFORMING

A typical hydroforming operation consists of applying proper combinations of internal pressure and axial feeding. There are many applications of tube hydroforming in the automotive industry and in household uses. This technology uses clamping devices such as mechanical presses, pressure intensifiers, hydraulic punches and control systems. There are various factors affecting the tube hydroforming process, such as, tube material and formability, friction, tube bending and pre-forming, and loading path (variation of internal pressure and axial feed with time). Hydroforming tubular components offer several advantages, including [37]:

a. Part consolidation.

b. Weight reduction through more efficient section design and tailoring of the wall thickness.

c. Improved structural strength and stiffness.

d. Lower tooling cost as a result of fewer parts.

e. Fewer secondary operations.

f. Tight dimensional tolerances and low spring-back.

g. Reduced scrap.

2.1 Current Applications

There are many applications of tube hydroforming in the automotive industry, and the aircraft industry [38]. Many companies in the automotive sector are experiencing great success with the process which can reduce weight, overall costs, and the number of parts per vehicle.

Current automotive applications are listed below [39].

a. Roof Headers

b. Instrument Panel Supports

c. Radiator Supports

d. Engine Cradles

e. Roof Rails

f. Frame Rails.

Other automotive applications include engine sub-frame, rear axle and exhaust manifolds.

Current applications of hydroforming in the automotive industry are:

a. The Chrysler Minivan "S" body instrument panel beam was the first high volume application for Pressure Sequence Hydroforming [40].

b. A hydroformed instrument panel reinforcement replaced a proposed three piece stamped and welded assembly resulting in a 3 pound weight reduction in the Ford Aerostar Instrument Panel [40].

c. The Ford CDW platform was the first to utilize a hydroformed engine cradle perimeter tube [40].

d. The redesigned 1994 Dodge Ram pickup truck includes the use of a hydroformed radiator closure assembly. Dodge replaced the conventional stamped and welded closure with one using hydroformed tubes resulting in 28 % fewer parts and 24% less weight for Dodge Dakota [40].

e. The Opel Vectra is equipped with an engine cradle assembly which employs a tube formed using the Pressure Sequence Hydroforming processes [40].

f. The release of the redesigned Jeep Grand Cherokee saw the third introduction of a hydroformed radiator closure for DaimlerChrysler [40].

Tube hydroforming is also used for the manufacturing of bathroom faucet spouts, aluminum riflescopes and steel panic bars.

2.2 THF Equipments

The major components of a hydroforming system are as follows [1] (Fig. 2-1):

a. Pressure or clamping devices,

b. Tooling,

c. Pressure system or intensifier,

d. Hydraulic cylinder and punches, and

e. Process control systems: computers, data acquisition, transducers, etc.
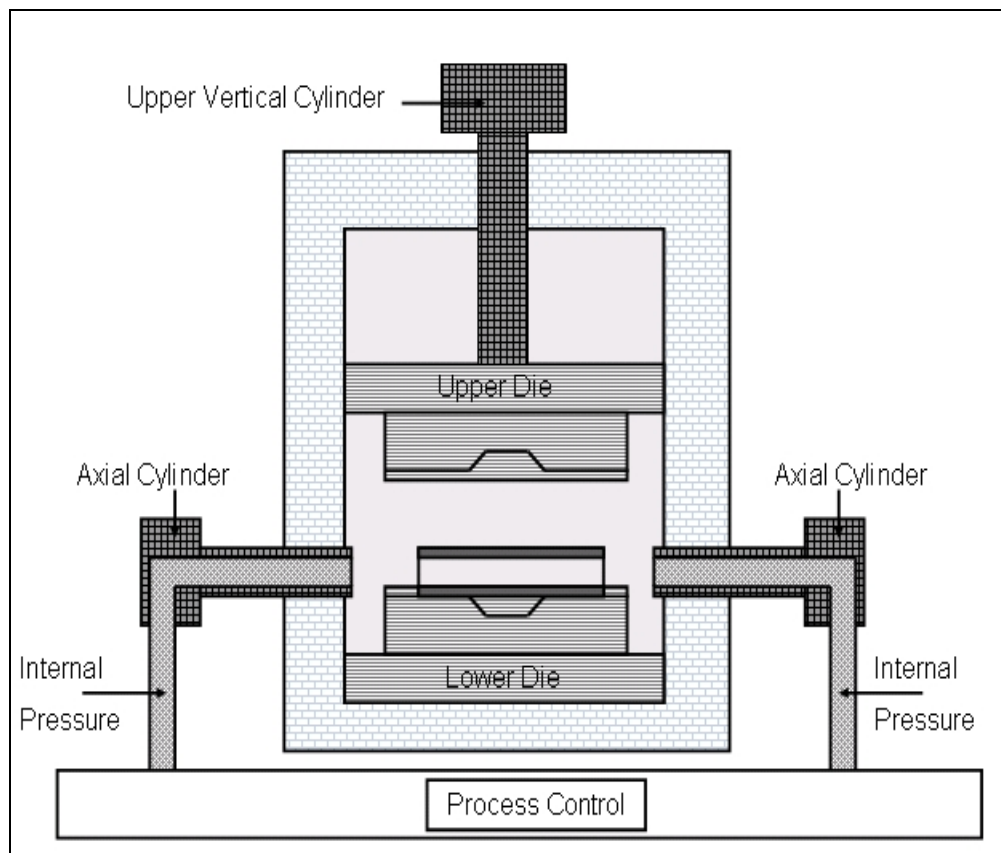
Figure 2-1: Major Components of a Hydroforming System

2.2.1   Presses or clamping devices

Tube Hydroforming (THF) process presses are used to open and close the die and to provide enough clamping load during the forming period to prevent elastic deflections and die separation. Tonnage of the press (or clamping device) is dependent on the required closing force [1]. Closing force is a function of the maximum internal pressure, part specifications and material. Large components with thick walls (i.e. chassis components) and intricate regions (i.e. small corner radii) need high closing forces up to 7000 - 8000 t [41].

In principle, a THF press or machine must have the following features [1]:

a. Appropriate die closing force,

b. Appropriate bed size to hold the dies,

c. Adjustable/movable axial punches with computer controlled positioning,

d. Adjustable/movable rams for counter forces with free and position control,

e. Optional: automatic work-piece handling, and

f. High pressure (2000 - 5000 bar) and fluid pumping capability with tight control.

2.2.2 Tooling

Hydroforming tooling consists of die holders, dies, inserts, punches, sealing systems and sometimes counter punches or movable inserts [1].

In general, the following are the main requirements for THF tooling [42 - 45]:

a. High strength against stresses due to large internal pressure and axial loading,

b. Good surface finish to minimize friction and increase formability,

c. Flexibility by interchangeable inserts,

d. Good guiding systems, and

e. Balanced design to minimize the closing force requirements.

2.2.3 Pressure System

The pressure system (pump, intensifier and control valves) are designed to provide the required pressure levels for a wide range of parts [1]. The applied pressure should have a range from 2000 bar (30 ksi) up to 10 000 bar (150 ksi) depending on the parts in consideration [46].

2.2.4 Hydraulic Cylinders and Punches

The axial punches are necessary to [1]:

a. Seal the end of the tube to avoid pressure losses and

b.   Feed material into expansion regions.

They should feed the material into the deformation zone in a controlled way and in coordination with internal pressure [1]. Counter punches are sometimes used on bulged or protrusion sections to avoid premature fracture by providing a controlled material flow. Axial cylinders are expected to generate forces of up to 7000 kN (700 t) while counter cylinder limits extend up to 2000 kN (200 t) [44].

2.3 Factors Affecting the Tube Hydroforming Process

This process requires the proper combination of part design, material selection, friction and application of internal pressure and axial feeding. Each of these components plays an important role in the success of the process and they have to be addressed during the process development stage.

2.3.1   Tube Material and Formability

Success of the hydroforming process significantly depends on the quality of the incoming tube. Material properties such as material composition, yield strength, ultimate tensile strength, percentage elongation and flow characteristics, and dimensions of the tube must be determined based on the final part requirements [47].

The required characteristics of tubular materials for manufacturing quality THF products are listed below [1].

a. High and uniform elongation,

b. High strain-hardening exponent,

c. Close mechanical and surface properties of weld line to the base material,

d. Good surface quality, free of scratches,

e. Close dimensional tolerances (thickness, diameter and shape),

f. Burr free ends; should be brushed, and

g. Tube edges perpendicular to the longitudinal axis.

Different testing methods have been used to determine the quality of tubing for purposes other than THF process [38]. These tests can be listed as follows:

a. Tensile test,

b. Expansion test,

c. Cone test, and

d. Bulge test.

Altan et al. [48] developed a methodology to determine the material properties of tubular blanks using a bulge test. The process for determining the material properties involves [48]:

a. Plastically deforming a tubular specimen,

b. Analytically determining the material properties, and

c. Using computer simulation to refine the analytically determined values.

2.3.2 Friction

There exists different tests for the determination of the coefficient of fricton (COF) for hydroforming of tubes. Schmoeckel et al. [49] identified different friction zones on a typical THF process depending on the effects of axial force, feeding and geometrical aspects. The surface pressure, sliding velocity and state of stress and strain were identified to be different in these zones as follows (Fig. 2-2): (a) guide zone, (b) transition zone and (c) expansion zone.
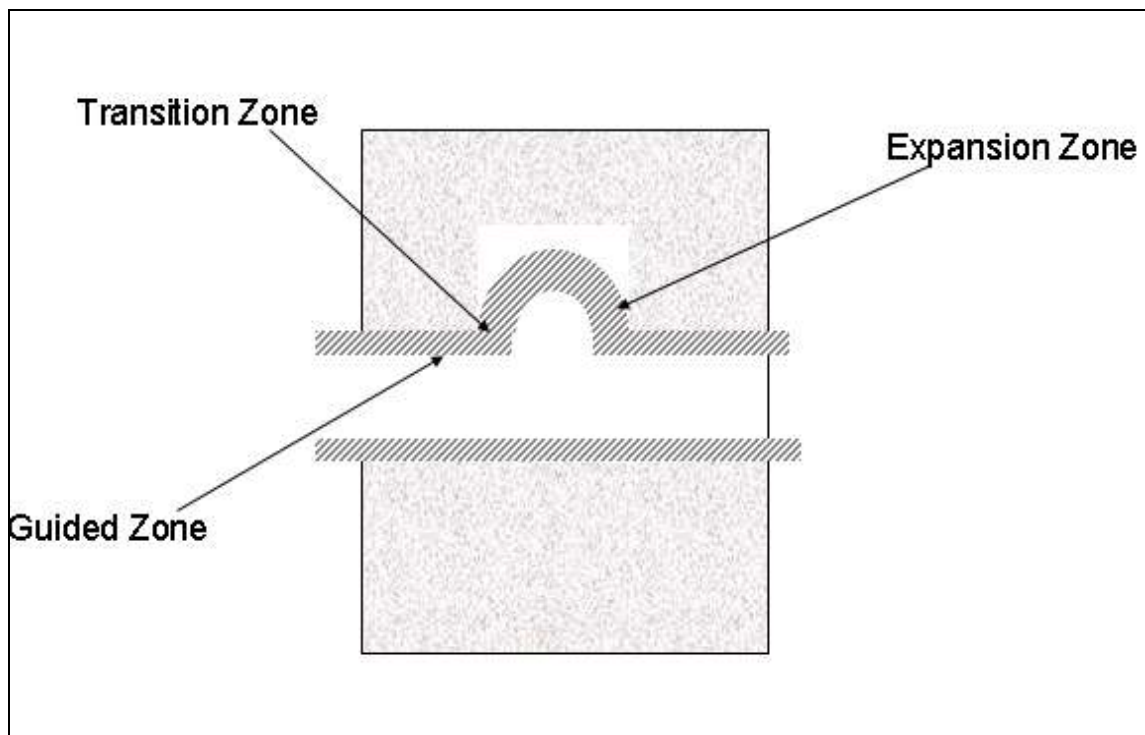
Figure 2-2: Different zones in tube hydroforming [38]

In order to investigate the influence of the above parameters in different zones of friction, Schmoeckel et al. [49, 50] used an experimental setup where a straight tube was expanded under internal pressure and pushed to investigate the friction conditions in guide zone only. Simultaneously, Dohmann [51] developed a different type of tooling which would permit investigation of friction in all zones.

Vollertsen et al. [52] mentioned the principles of COF measurement and developed a new principle based on upsetting of tubes to determine the coefficient of friction. Vollertsen et al. stated that friction plays an increasing role in controlling the tube thickness [52]. They stated that since the contact pressure is high and the contact surface is large, the friction forces make a dominant portion of the punch forces. Thus, it becomes important to determine the coefficient of friction in order to enable the development of strategies for a reduction of the coefficient of friction.

2.3.3 Tube Bending and Pre-forming

In many applications the tube is pre-bent to the approximate contours of the part before the hydroforming operation. Therefore, limits of the bending operation should be taken into consideration during the product design stage [47]. There are several methods that can be used in tube bending. Some of these methods are compression bending, press bending, three-roll bending, hydro-bending and rotary draw bending [53, 54]. The most commonly used bending method for hydroforming is rotary draw bending (Fig. 2-3). In

rotary draw bending the tube is locked to the bend die by the clamp. As the bend die rotates, the pressure die advances with the tube. In this process, a mandrel may be used (depending on the bend die and tube geometry) to prevent excessive collapse and wrinkling in the bend region. Rotary draw bending is performed in CNC-controlled benders.
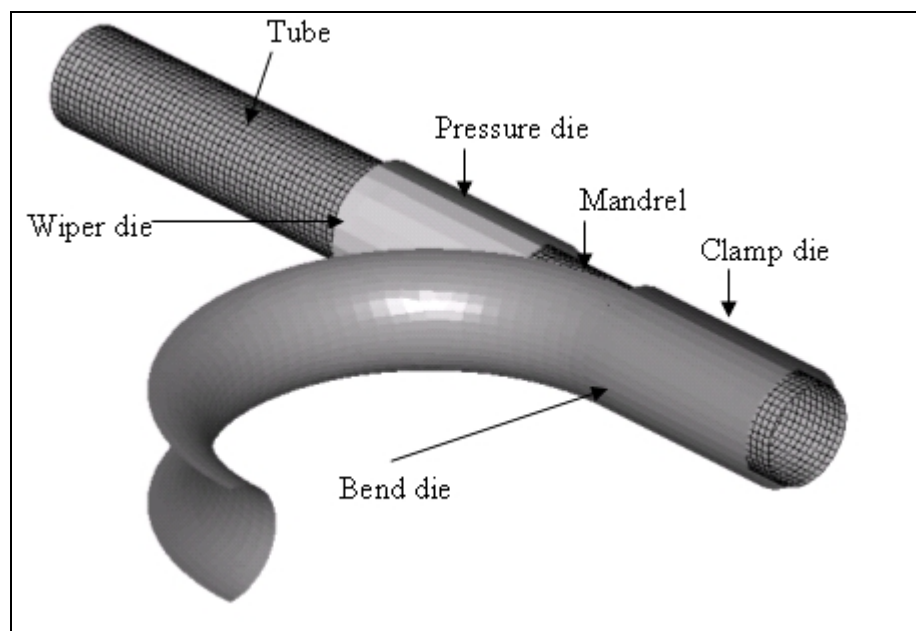
Figure 2-3: Rotary Tube Bending

2.3.4   Loading Path

The loading curves (variation of internal pressure and axial feed with time) forms the most important part of THF. In principle, three failure types are encountered in tube

hydroforming: buckling, wrinkling and fracture (bursting) [35]. Wrinkling and fracture are shown in Fig. 2-4.
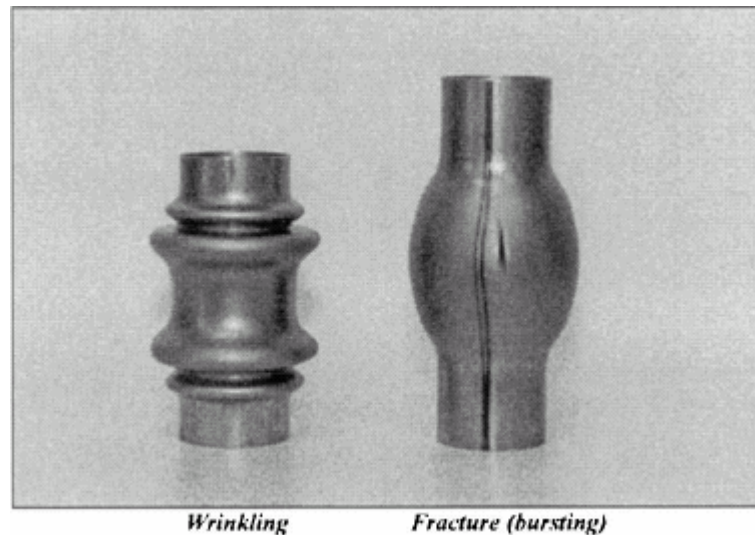
Figure 2-4: Failure Modes in Tube Hydroforming – Wrinkling and Bursting [35]

Instability modes, which limit the extent of formability in THF process, occur when the stress and strain state in a part reach a critical level such that equilibrium cannot be sustained any longer between external forces applied and the internal resistance of the material (i.e. strength) [20].

The hydroforming operation is comprised of two stages: free forming and calibration. The portion of deformation in which the tube expands without tool contact is called free forming. As soon as tool contact is established, the calibration starts. During calibration,

no additional material is fed into the expansion zone by the axial cylinders. The tube is forced to adopt the tool shape by increasing the internal pressure [35].

Buckling or wrinkling occurs when the axial compressive stress on an element of a part exceeds the strength of the material. Buckling in THF process takes during the initial stages of deformation when the strain level is very small. It usually occurs in long tubes with relatively thick walls (i.e. low D/t ratios) [20]. Wrinkling, on the other hand, is observed during both the initial and the intermediate stages of forming in the form of symmetric corrugations on the both long and short tubes with relatively thin walls (i.e. high D/t ratios) [20]

The loading curves (variation of internal pressure and axial feed with time) have to be designed to produce a controlled deformation, avoiding any of the failure types that are encountered in tube hydroforming (buckling, wrinkling and fracture). Many researchers have presented the theoretical and the practical work about the estimation of load parameters for the tube hydroforming using various techniques [20, 35, 36].

2.4 Finite Element Modeling of Tube Hydroforming Process

Finite element modeling provides a powerful tool for design engineers. Since the main interest here is to demonstrate the merits of dual tube hydroforming, simulation of the tube hydroforming with no external counter pressure was first conducted to establish a

baseline for comparison. The development of a validated FEA is required to access accurate results. The simulation technique is validated based on the experimental data presented by Hutchinson [55] and MacDonald et. al. [56].

Hutchinson performed the experiments for cylindrical tubes with outer diameter of 24.12 mm, length of 107.00 mm, and wall thickness of 1.37 mm and 1.03 mm. In the simulations, a finite element model of the cylindrical tube (24.12 mm outer-diameter, 107 mm length) with quadrilateral shell element was constructed to simulate the cross joints bulge forming. The discretized quarter model is as shown in Fig. 2-5.
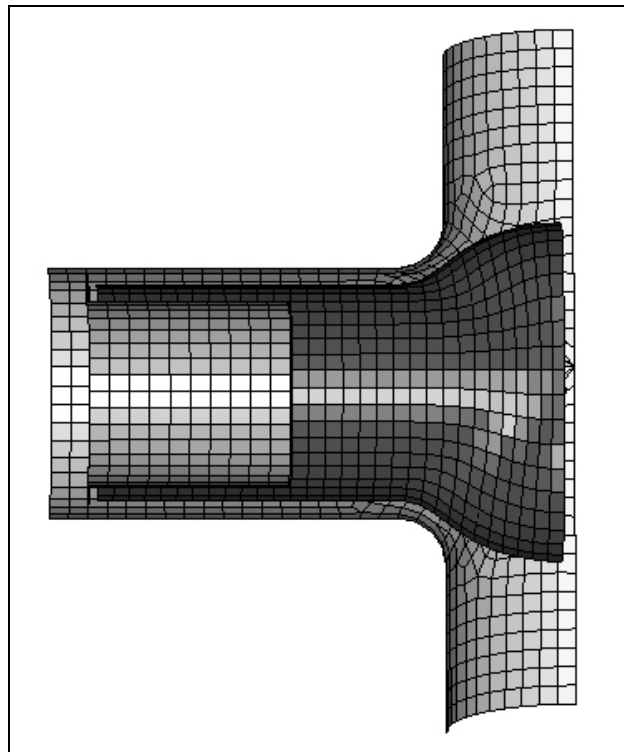
Figure 2-5: Finite Element Model Showing Tube, Die and Punch for Tube Hydroforming

The die and the punch were considered to be rigid by the analysis and each was modeled as a rigid surface. A master-slave contact approach was used in the analysis where the die was considered as the master surface and the surface of the tube was considered as the slave surface. While the die and the punch were assigned rigid material properties, the tube was assigned a piecewise linear elastic-plastic material model. The internal hydraulic pressure was applied as a uniformly distributed load to the tube inner surface. The axial feed was applied as a prescribed displacement of the punch as a linearly increasing function of the time. Details of the finite element modeling are provided in Appendix A (p. 94) and the input deck information is in Appendix B (p. 102). The material properties used are shown in Table 2-1 [56].

Table 2-1: Material Properties for Copper

Material Properties	
Young's modulus	124×10^3 MPa
Yield strength	160 MPa
Tangent modulus	925 MPa
Poisson's ratio	0.3
Density	8.9×10^{-6} kg/mm^3
Ultimate tensile strength	330 MPa

In most of the commercial tube hydroforming processes axial displacement (stroke controlled) is used instead of axial force. Finite element simulations were also carried out using axial displacement as the loading condition. However, Hutchinson performed the experiments with axial force (instead of axial displacement) for various internal

pressures. The graph between the Ratio of Final to Initial Tube Length (in %) versus Compressive Axial Load (in kN) was used to convert the axial force to approximate axial feed [55]. For a particular axial force, the corresponding ratio of final to initial tube length was multiplied to the initial length of the tube. Hence, final length of the tube can be calculated as a result of the applied axial force. This final length of the tube was subtracted from the initial tube length and divided by 2 to obtain the axial stroke.

The validation was performed for the tube wall thickness of 1.03 mm. The axial force of 43 kN in the experiment was found equivalent to 2 mm axial stroke. The internal pressure of 24.1 MPa, which is known from the experiments conducted by Hutchinson [55], was used for simulation. The loading path is shown in Fig 2-6. The final values of the loading path in Fig. 2-6 are known from the experiments conducted by Hutchinson [55] and the intermediate points are known from the simulations conducted by MacDonald [56]. While recording the percentage thinning versus the bulge height in one of the runs (for tube thickness of 1.03 mm), the simulation result was close to the experimental result shown in Fig. 2-7.
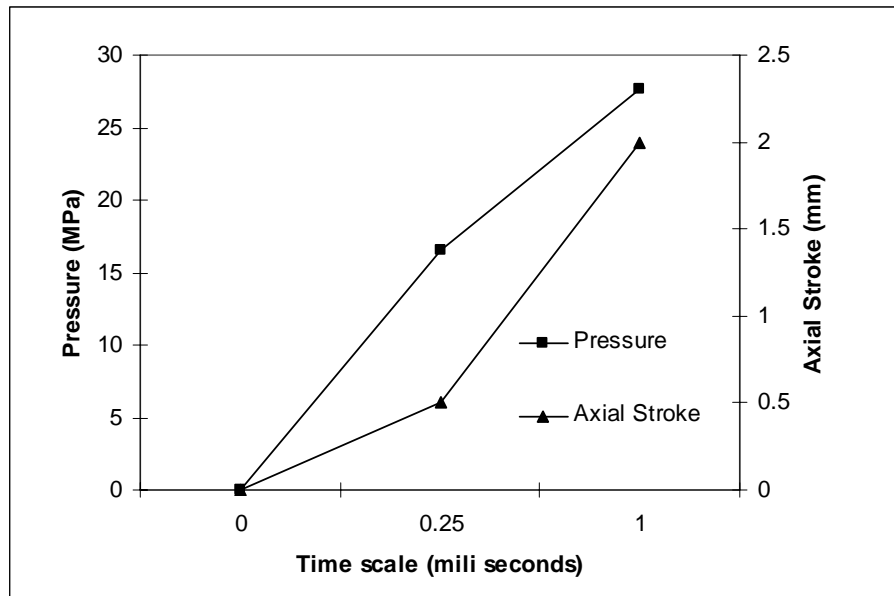
Figure 2-6: Loading Path for Tube of Wall Thickness 1.03 mm [55, 56]
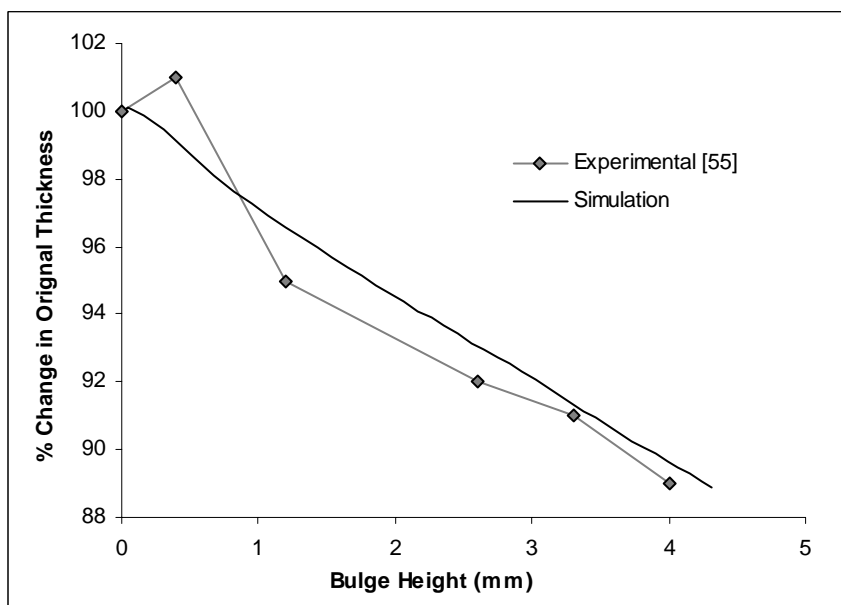
Figure 2-7: Comparison of Deformation for Cross Joints Bulge Forming for Tube
Wall Thickness of 1.03 mm

The validation was also performed for the tube thickness of 1.37 mm. The axial force of 85 kN in the experiment was found to be close to 12.00 mm axial stroke. The bulge heights and the corresponding percentage thinning were obtained for the various internal pressures and keeping the same axial stroke (for tube of 1.37 mm thickness). The simulation runs 1 through 3 represent internal pressures of 34.50 MPa, 41.40 MPa, and 48.30 MPa given by Hutchinson and loading path are shown in Fig. 2-8. The final values of the loading path in the Fig. 2-6 were known from the experiments conducted by Hutchinson [55] and the intermediate points were known from the simulations conducted by MacDonald [56]. As shown in the Table 2-2, the bulge heights and the percentage thinning obtained from the simulations agree well with the experimental results. The possible reasons for the slight disagreement could be because of the material model (the tubular material properties used in the simulations were taken from the compression test by MacDonald [56]), the size of the mesh, the coefficient of friction, and the exact loading path.

This validated finite element model was used for all the simulations for the present work. The material properties used were the same as used in the validation unless stated otherwise.
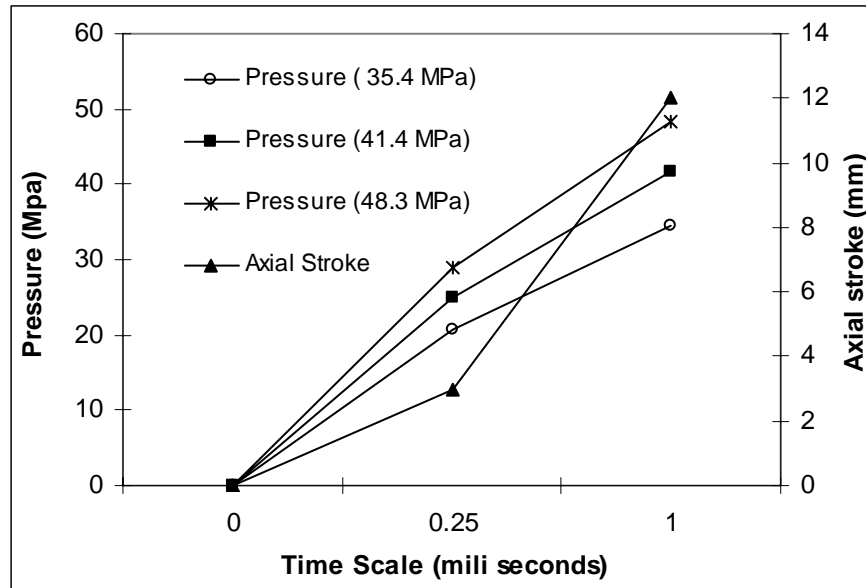
Figure 2-8: Loading Path for Tube of Wall Thickness 1.37 mm [55, 56]

Table 2-2: Comparison of Bulge Heights and Percentage Thinning Obtained for Various
Simulations with Experimental Results for Tube Thickness of 1.37 mm

Internal Pressure (MPa)	Bulge Height (mm)		% Thinning	
	Experimental [55]	Simulation	Experimental [55]	Simulation
35.4	8.50	8.46	3.00	2.38
41.4	10.00	10.17	7.00	7.79
48.3	11.50	11.00	12.00	11.68

CHAPTER III

MODELING OF DUAL HYDROFORMING

Tube deformation is controlled by 'gradually' increasing the internal pressure during the application of axial load (Fig. 3-1). The stress state at a given time and location varies with the process history, and the design and control of the load paths. In dual hydroforming an additional process parameter, counter-pressure is added to achieve controlled deformation (Fig. 3-1). The dual hydroforming process will have a different stress state at a given time and location as compared to tube hydroforming.
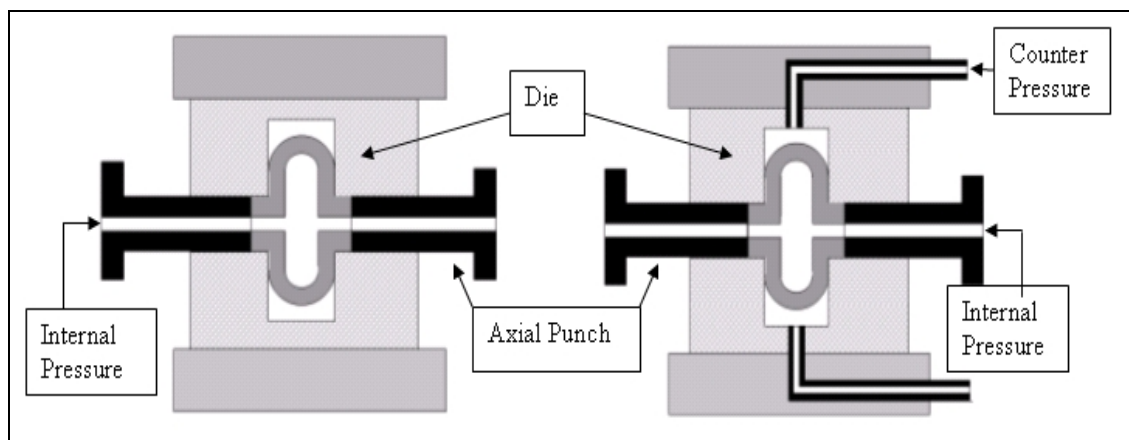
Figure 3-1: THF and DHF

Tube hydroforming and dual hydroforming will have different stress and strain state in the part. This will result in different wall thinning. The stress and the strain state at the mean diameter of the tube for tube hydroforming can be predicted using the analytical model developed by Ahmed et al [32]. To predict the stress and the strain state at the mean diameter of the tube for dual hydroforming a counter pressure term (p_o) was added to the model already developed by Ahmed et al [32]. The model was developed using the vonMises criterion instead of the Tresca criterion.

3.1 Analytical Model

The stress and the strain state for tube hydroforming and dual hydroforming will be compared at the mean diameter of the tube. Also, the thinning comparison between the tube hydroforming and the dual hydroforming will be made at the same bulge height. The comparison will be made for the condition that the hoop strain is zero. The zero hoop strain implies that there is no change in the mean diameter of the tube. The comparison will be made at this instantaneous point. Cylindrical coordinate system is chosen with r for the radial direction, θ for the hoop direction, and z for the axial direction (Fig. 3-2).
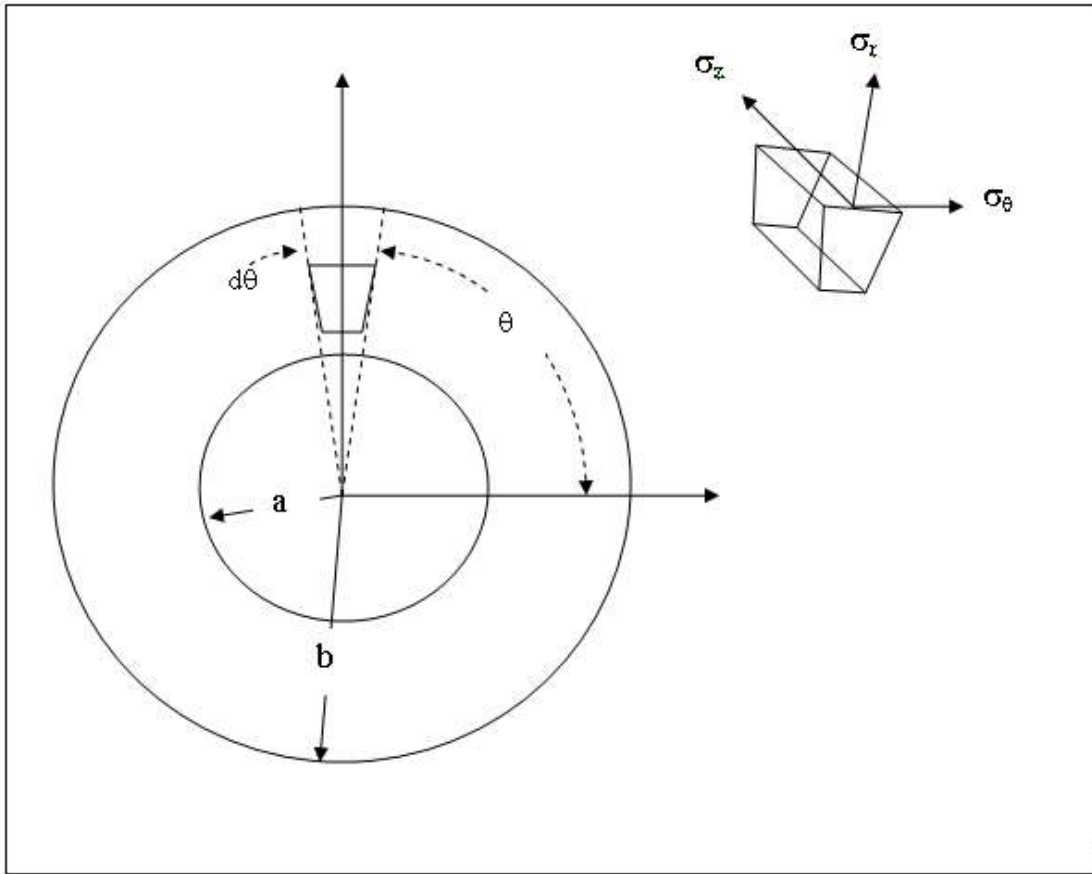
Figure 3-2: Thin-walled Tube in Cylindrical Coordinates

3.1.1 Stress and Strain State at Mean Diameter of Tube

A straight tube is considered having internal radius '*a*' and outer radius '*b*'.

Let t_o be the initial thickness.

As reported by Ahmed et al., the punches enter a length of x_o at each end of the tube and the unconstrained length is x [32] (Fig. 3-3).
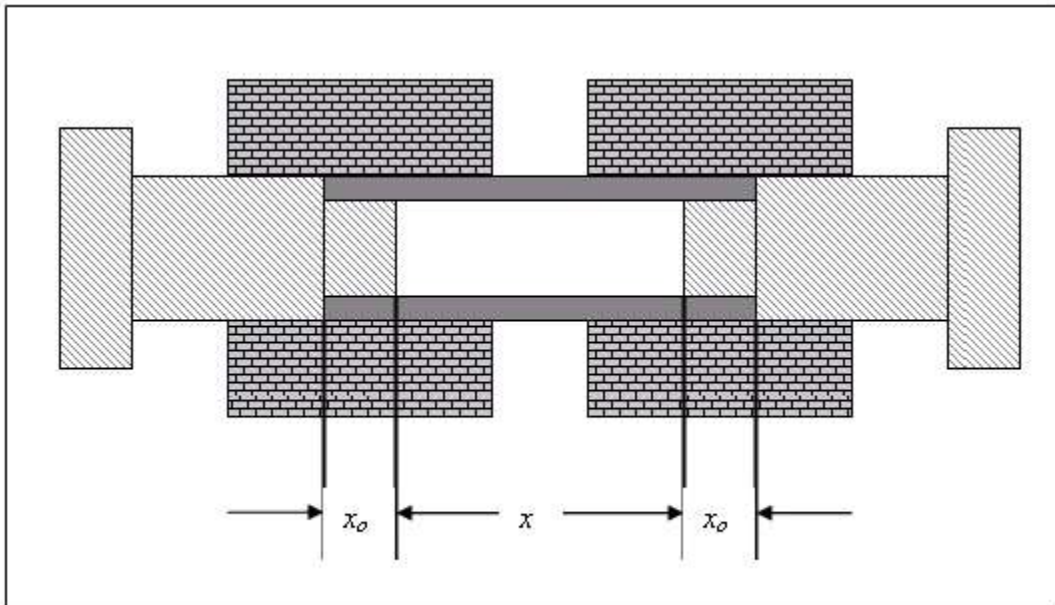
Figure 3-3: Tube under Bulging

The analysis by Ahmed et al. was based on the assumption that the mean diameter of the tube will not change significantly i.e. zero strain in the hoop direction (ε_θ= 0) [32].

Plane strain condition is considered where ε_θ= 0, the volume constancy would give ε_t = -ε_z. The deviatoric stress, $\sigma_\theta^{'} = 0$.

The normal axial stress, $\sigma_\theta = \dfrac{1}{2}\left(\sigma_r + \sigma_z\right)$ (3-1)

For an element within the deformation zone, the equilibrium of the forces in the radial direction gives [32],

$$\frac{d\sigma_r}{dr} + \frac{\sigma_r - \sigma_\theta}{r} = \frac{-2mk}{x} \tag{3-2}$$

where, m is the friction factor and k is the shear strength.

The equation (3-2) is solved to obtain the stress and the strain condition at the mean diameter of the tube as shown in Fig. 3-4. Details of the solution for equation (3-2) are given in Appendix C.
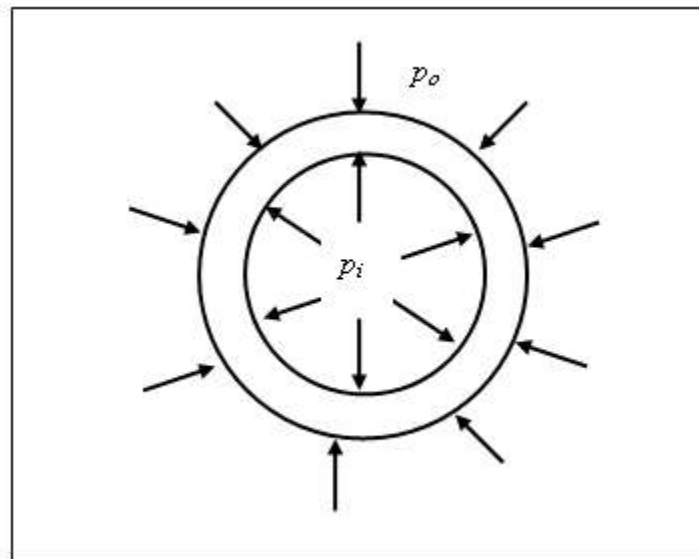
Figure 3-4: Tube with Internal and External Pressure

At $r = a$, $\sigma_{ra} = -p_i$, where $-p_i$ is the hydraulic pressure at the inner wall of the tube (Fig 3-4).

The axial stress at the inside surface of the deformation zone at radius $r = a$ is given by the equation (3-8), whereby

$$\sigma_{za} = \sigma_{ra} - \frac{2}{\sqrt{3}}\sigma_{yp} = -p_i - \frac{2}{\sqrt{3}}\sigma_{yp} \tag{3-3}$$

The radial stress at the outer surface of the tube within the deformation zone is σ_{rb} at $r = b$

$$\sigma_{rb} = -p_i - \frac{\sigma_{yp}}{\sqrt{3}r}\ln\frac{a}{b} - \frac{2m\sigma_{yp}(a-b)}{\sqrt{3}x} - p_o \tag{3-4}$$

The axial stress at the outside surface of the deformation zone at radius $r = b$ is given by the equation (3-8), whereby

$$\sigma_{zb} = \sigma_{rb} - \frac{2}{\sqrt{3}}\sigma_{yp} = -p_i - \frac{\sigma_{yp}}{\sqrt{3}r}\ln\frac{a}{b} - \frac{2m\sigma_{yp}(a-b)}{\sqrt{3}x} - p_o - \frac{2}{\sqrt{3}}\sigma_{yp} \tag{3-5}$$
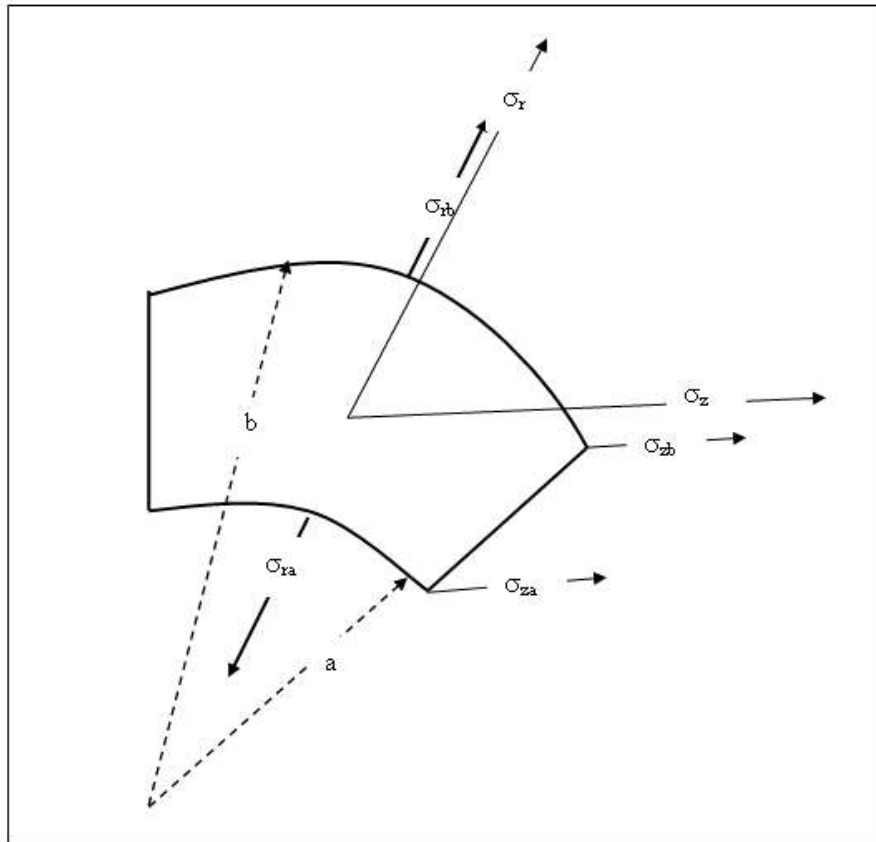
Figure 3-5: Radial and Axial Stress System

From the Fig. 3-5, the stress state at the mean diameter of the tube is given by following equations.

$$\sigma_r = \sigma_{rb} - \sigma_{ra}$$
$$\sigma_z = \frac{1}{2}\left(\sigma_{za} + \sigma_{zb}\right)$$
$$\sigma_\theta = \frac{1}{2}\left(\sigma_r + \sigma_z\right)$$

(3-6)

Using vonMises criterion the effective stress is calculated by using

$$\overline{\sigma} = \frac{1}{\sqrt{2}}\left[\left(\sigma_r - \sigma_\theta\right)^2 + \left(\sigma_\theta - \sigma_z\right)^2 + \left(\sigma_z - \sigma_r\right)^2\right]^{\frac{1}{2}}$$

Once the effective stress is known, effective strain can be calculated by

$$\overline{\sigma} = K\overline{\varepsilon}^n$$

From vonMises criterion for the effective strain,

$$\overline{\varepsilon} = \left[\frac{2}{3}\left(\varepsilon_t^2 + \varepsilon_\theta^2 + \varepsilon_z^2\right)\right] \tag{3-7}$$

Therefore, using equation (3-7) at $\varepsilon_\theta = 0$ and $\varepsilon_t = -\varepsilon_z$, ε_t can be calculated.

Hence the instantaneous thickness (t_i) can be calculated using, $\varepsilon_t = \ln\dfrac{t_i}{t_o}$.

3.1.2   Results and Discussion

To demonstrate the effect of counter pressure on the thickness change and the estimation of axial force, the following example is considered (Table 3-1).

Table 3-1: Properties of a Tube

Inner radius, mm	a	12.06
Outer radius, mm	b	13.43
Initial thickness, mm	t_o	1.37
Length of tube, mm	L	107
Punches enter a length, mm	x_o	10
Unconstrained length, mm	x	87
Coefficient of friction	m	0.1
Internal pressure, MPa	p_i	40
Counter pressure, MPa	p_o	7
Yield Strength, MPa	σ_{yp}	160
Strength coefficient, MPa	K	500
Strain hardening exponent, MPa	n	0.35

Using the methodology derived earlier, the following parameters were calculated for tube hydroforming and dual hydroforming.

Tube Hydroforming (without counter pressure)

$\sigma_{ra} = -p_i, = -40$ MPa

$$\sigma_{rb} = -p_i - \frac{\sigma_{yp}}{\sqrt{3}r} \ln\frac{a}{b} - \frac{2m\sigma_{yp}(a-b)}{\sqrt{3}x} - p_o = -50.230 MPa$$

$$\sigma_{za} = \sigma_{ra} - \frac{2}{\sqrt{3}}\sigma_{yp} = -p_i - \frac{2}{\sqrt{3}}\sigma_{yp} = -224.752 MPa$$

$$\sigma_{zb} = \sigma_{rb} - \frac{2}{\sqrt{3}}\sigma_{yp} = -p_i - \frac{\sigma_{yp}}{\sqrt{3}r}\ln\frac{a}{b} - \frac{2m\sigma_{yp}(a-b)}{\sqrt{3}x} - p_o - \frac{2}{\sqrt{3}}\sigma_{yp} = -234.982 MPa$$

$$\sigma_r = \sigma_{rb} - \sigma_{ra} = -10.230 MPa$$

$$\sigma_z = \frac{1}{2}(\sigma_{za} + \sigma_{zb}) = -229.867 MPa$$

$$\sigma_\theta = \frac{1}{2}(\sigma_r + \sigma_z) = -120.049 MPa$$

$$\overline{\sigma} = \frac{1}{\sqrt{2}}\left[(\sigma_r - \sigma_\theta)^2 + (\sigma_\theta - \sigma_z)^2 + (\sigma_z - \sigma_r)^2\right]^{1/2} = 190.211 MPa$$

Using, $\overline{\sigma} = K\overline{\varepsilon}^n$

$\overline{\varepsilon} = 0.0632$

From vonMises criterion for effective strain,

$$\overline{\varepsilon} = \left[\frac{2}{3}(\varepsilon_t^2 + \varepsilon_\theta^2 + \varepsilon_z^2)\right] \quad (26)$$

and $\varepsilon_\theta = 0$ and $\varepsilon_t = -\varepsilon_z$,

$$\varepsilon_t = -0.0547$$

$$\varepsilon_t = \ln\frac{t_i}{t_o} \Rightarrow t_i = 1.2970mm$$

Dual Hydroforming (with counter pressure of 7 MPa)

$\sigma_{ra} = -p_i, = -40$ MPa

$$\sigma_{rb} = -p_i - \frac{\sigma_{yp}}{\sqrt{3}r}\ln\frac{a}{b} - \frac{2m\sigma_{yp}(a-b)}{\sqrt{3}x} - p_o = -57.230MPa$$

$$\sigma_{za} = \sigma_{ra} - \frac{2}{\sqrt{3}}\sigma_{yp} = -p_i - \frac{2}{\sqrt{3}}\sigma_{yp} = -224.752MPa$$

$$\sigma_{zb} = \sigma_{rb} - \frac{2}{\sqrt{3}}\sigma_{yp} = -p_i - \frac{\sigma_{yp}}{\sqrt{3}r}\ln\frac{a}{b} - \frac{2m\sigma_{yp}(a-b)}{\sqrt{3}x} - p_o - \frac{2}{\sqrt{3}}\sigma_{yp} = -241.982MPa$$

$$\sigma_r = \sigma_{rb} - \sigma_{ra} = -17.230MPa$$

$$\sigma_z = \frac{1}{2}(\sigma_{za} + \sigma_{zb}) = -233.367MPa$$

$$\sigma_\theta = \frac{1}{2}(\sigma_r + \sigma_z) = -125.299MPa$$

$$\overline{\sigma} = \frac{1}{\sqrt{2}}\left[(\sigma_r - \sigma_\theta)^2 + (\sigma_\theta - \sigma_z)^2 + (\sigma_z - \sigma_r)^2\right]^{1/2} = 187.180MPa$$

Using, $\overline{\sigma} = K\overline{\varepsilon}^n$

$$\overline{\varepsilon} = 0.0604$$

From vonMises criterion for effective strain,

$$\overline{\varepsilon} = \left[\frac{2}{3}(\varepsilon_t^2 + \varepsilon_\theta^2 + \varepsilon_z^2)\right]$$

and $\varepsilon_\theta = 0$ and $\varepsilon_t = -\varepsilon_z$,

$$\varepsilon_t = -0.0523$$

$$\varepsilon_t = \ln\frac{t_i}{t_o} \Rightarrow t_i = 1.3002mm$$

Dual hydroforming results in a different stress and a strain state at the mean diameter of

the tube. This resulted in different thickness and percentage thinning as given in

Table 3-2.

Table 3-2: Difference in Stress and Strain State and Thickness for THF and DHF

	Tube Hydroforming	Dual Hydroforming
Axial Stress, σ_z (MPa)	-229.867	-233.367
Radial Stress, σ_r (MPa)	-10.230	-17.230
Hoop Stress, σ_θ (MPa)	-120.049	-125.299
Effective Stress, $\bar{\sigma}$ (MPa)	190.211	187.180
Effective Strain, $\bar{\varepsilon}$	0.0632	0.0604
Thickness, t_i (mm)	1.2970	1.3002
Percentage Thinning, %	5.32	5.09

Tube hydroforming produced a thinning of 5.32 % while dual hydroforming produced is

5.09 %. The new process parameter enabled favorable tri-axial stress state during the

deformation. The counter pressure provided the back support to the tube material and

hence produced the lesser thinning. Inversely, larger tube expansion can be achieved for

the given amount of thinning.

3.2 Finite Element Analysis –Thinning

The internal hydraulic pressure of 40 MPa was applied as a uniformly distributed load to the tube inner surface. The internal pressure was introduced as a linearly increasing function of time. The axial stroke of 12 mm was applied as a prescribed displacement of the punch. The external counter pressure of 7 MPa was also applied as a linearly increasing function of time. Two different loading conditions were analyzed. The initial run was conducted without applying the external counter pressure (Load Pattern 1 shown in Fig. 3-6 (THF)). Keeping the same internal pressure and axial feed curves, the analysis followed with the application of external counter pressure (Load Pattern 2 shown in Fig. 3-7 (DHF)).
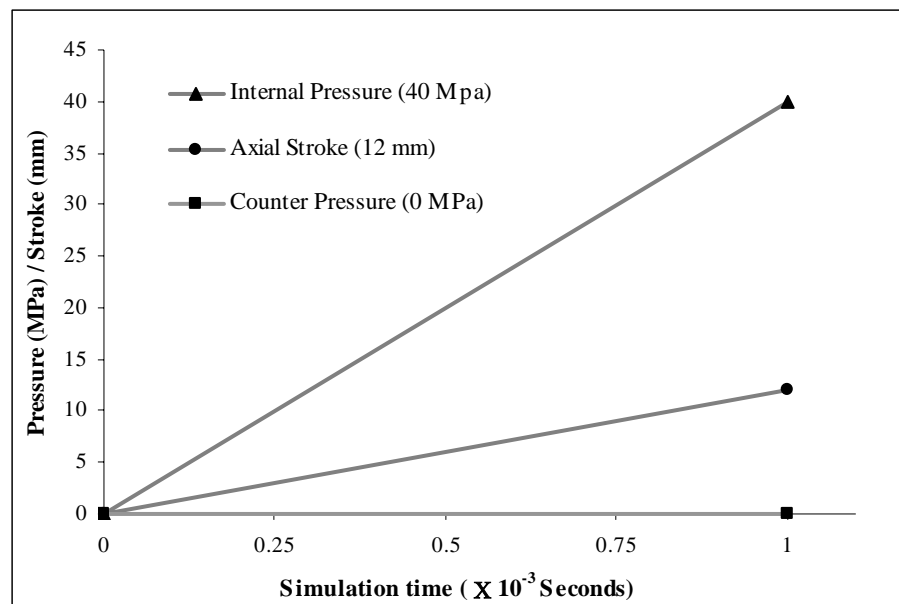
Figure 3-6: Load Pattern 1 – Without Counter Pressure
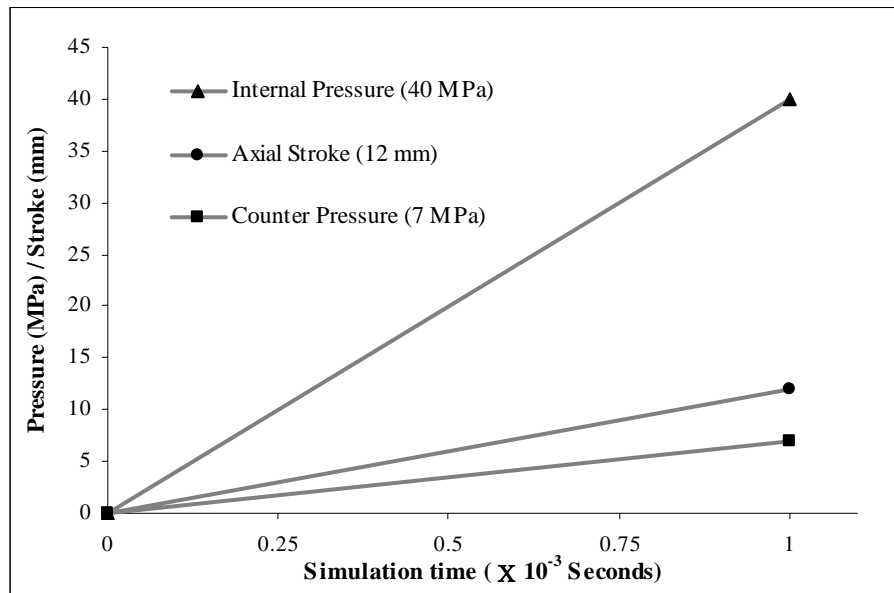
Figure 3-7: Load Pattern 2 – With Counter Pressure

Monitoring the elements that end up with the minimum thickness in these runs,

Figure 3-8 shows the thickness history of these elements versus bulge height. The

simulations resulted in different bulge heights. However, the simulations showed that at

the same bulge height different counter pressure load paths could lead to different

minimum thickness of the tube. As shown in the Table 3-3, for a bulge height of 7.9 mm

dual hydroforming resulted in less thinning. On the other hand for a given minimum

thickness, different counter pressures result in different degrees of tube expansion.
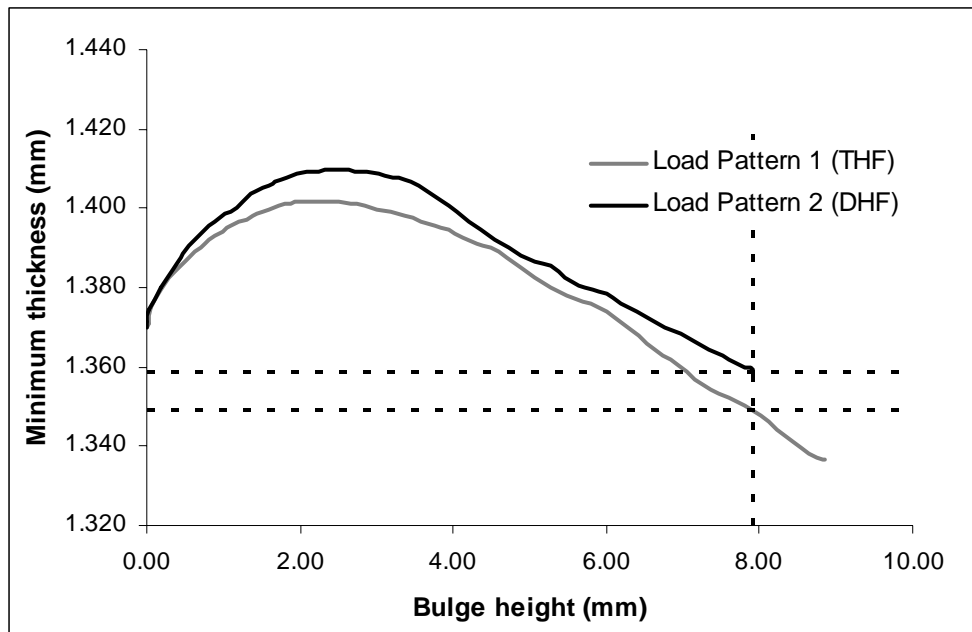
Figure 3-8: Deformation Characteristics for THF and DHF

Table 3-3: Bulge Height, Minimum Thickness and Percentage Thinning for THF and DHF

	Bulge Height (mm)	Minimum thickness (mm)	Percentage Thinning
Load Pattern 1, THF	7.90	1.349	1.53
Load Pattern 2, DHF	7.90	1.359	0.80

Thus, it can be concluded that the different and the favorable stress and strain distributions resulted in less thinning in the case of dual hydroforming. Figure 3-9 and Fig. 3-10 show the distribution of the effective stress and the strain for the tube and the dual hydroforming respectively.
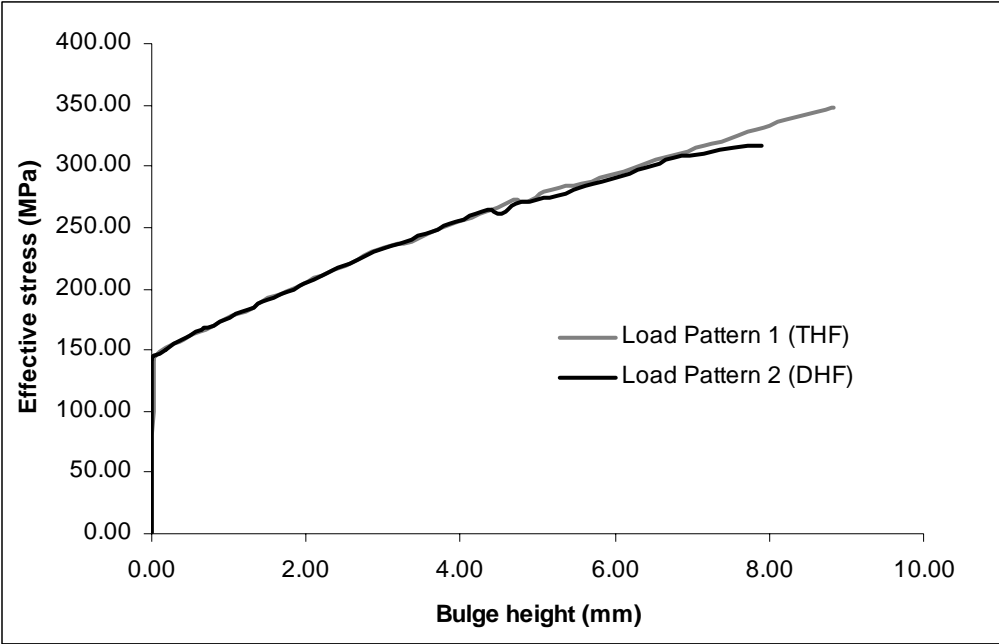
Figure 3-9: Effective Stress Plot for THF and DHF
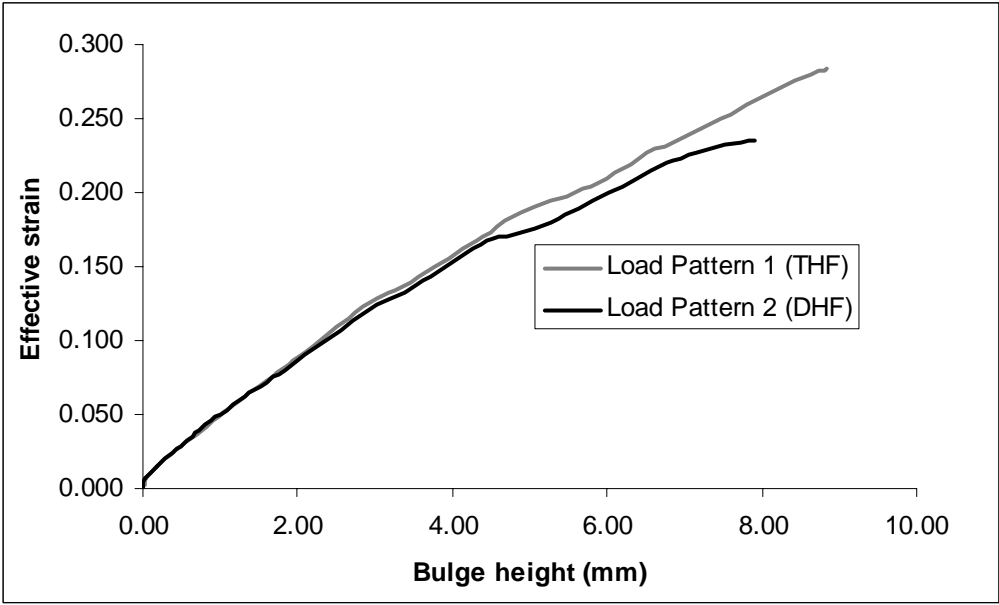
Figure 3-10: Effective Strain Plot for THF and DHF

CHAPTER IV

PLASTIC INSTABILITY IN DUAL HYDROFORMING

Successful tube hydroforming requires the bulging to take place without causing any type of instability like bursting, necking, wrinkling or buckling. Excessive pressure without sufficient axial feed will cause the tube to fracture, while excessive application of axial force will lead to wrinkling of the tube. The earlier chapter showed that there is less thinning in the case of dual hydroforming due to a different stress and strain state. But less thinning does not imply that the tube will not fracture as necking depends on the plastic instability criterion. The effect of applying counter pressure on the plastic instability of thin walled tubes with only internal pressure and combination of internal pressure and independent axial loading is considered. This chapter establishes a plastic instability criterion for dual hydroforming process based on the method used by Mellor [22]. The effect of different boundary conditions on the plastic instability criterion will also be emphasized by considering the following cases:

a.   Internal Pressure (THF)

b.   Internal Pressure and Axial Feed (THF)

c.   Internal Pressure and Counter Pressure (DHF)

d.   Internal Pressure, Axial Feed and Counter Pressure (DHF)

This chapter contains only the important equations. The detailed analysis and derivations is given in Appendix D.

4.1 Plastic Instability

The methodology used by Mellor to determine the plastic instability criterion is outlined below [22]:

a. The system is stable as long as the increase in load carrying capacity due to work hardening at any incipient neck can compensate for the decrease in load-carrying capacity due to reduction in cross-sectional area.

b. This corresponds to maximum load condition, when an incipient neck will continue to grow and the system then becomes unstable.

Assumptions considered by Mellor in the instability analysis are [22]:

a. Elastic strains are negligible compared with the plastic strains.

b. Material is assumed isotropic and remains isotropic under the imposed strain.

The above method is illustrated by establishing a plastic instability criterion for a uniaxial tensile test as reported by Mellor [22]. The stress σ_1 in the longitudinal direction is given by,

$$\sigma_1 = \frac{F}{A} \tag{4-1}$$

where, F is the applied load over a cross-sectional area A.

Let a small additional longitudinal strain $\delta\varepsilon_1$ be imposed when the stress is σ_1.

From equation (4-1), work-hardening requires that the load F be increased by an amount

$$A\frac{d\sigma_1}{d\varepsilon_1}\delta\varepsilon_1 \qquad\qquad (4\text{-}2)$$

On the other hand, reduction of cross-sectional area corresponds to a reduction in load of

$$\sigma_1\frac{dA}{d\varepsilon_1}\delta\varepsilon_1 \qquad\qquad (4\text{-}3)$$

An "incipient neck" is formed at some part of the bar [22]. The system is stable as long as the increase in load carrying capacity due to work hardening at any incipient neck can compensate for the decrease in load-carrying capacity due to reduction in cross-sectional area [22].

Therefore, instability occurs when,

$$A\frac{d\sigma_1}{d\varepsilon_1}\delta\varepsilon_1 + \sigma_1\frac{dA}{d\varepsilon_1}\delta\varepsilon_1 = 0 \qquad\qquad (4\text{-}4)$$

The above equation yields, $\dfrac{1}{\overline{\sigma}}\dfrac{d\overline{\sigma}}{d\overline{\varepsilon}} = 1$ $\qquad\qquad (4\text{-}5)$

But $\dfrac{1}{\overline{\sigma}}\dfrac{d\overline{\sigma}}{d\overline{\varepsilon}} = \dfrac{1}{z}$ $\qquad\qquad (4\text{-}6)$

where z is the sub-tangent modulus as shown in Fig 4-1 and $\overline{\varepsilon} = nz$.
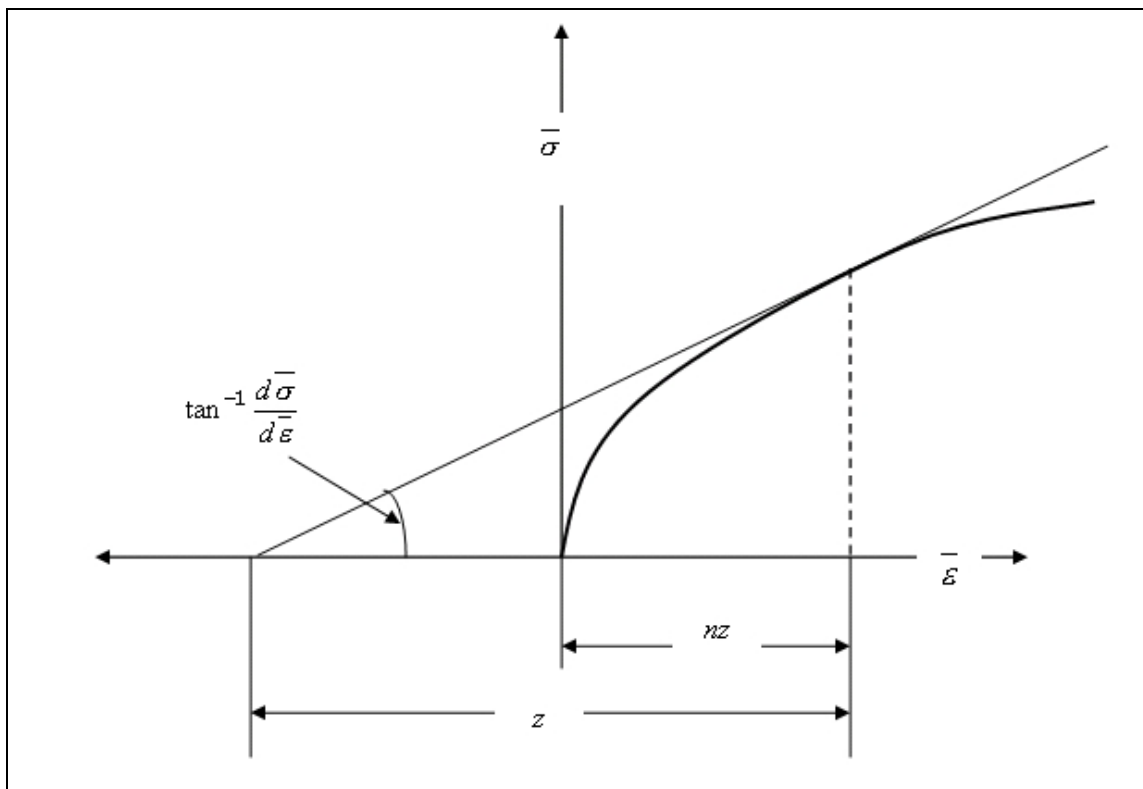
Figure 4-1: Sub-tangent Modulus z

Therefore, the critical strain for the uniform tensile test from equation (4-6)

$$\bar{\varepsilon} = \varepsilon_1 = n(1) = n \qquad \qquad (4\text{-}7)$$

4.2 Plastic Instability - Thin Walled Tubes

As plastic instability criterion has to be established for dual hydroforming (additional counter pressure), a force balance analysis is done in the radial direction for the thin

walled tubes (Fig. 4-2). A section in cylindrical co-ordinate system is considered here where r is for radial, θ for hoop direction and z for axial direction.
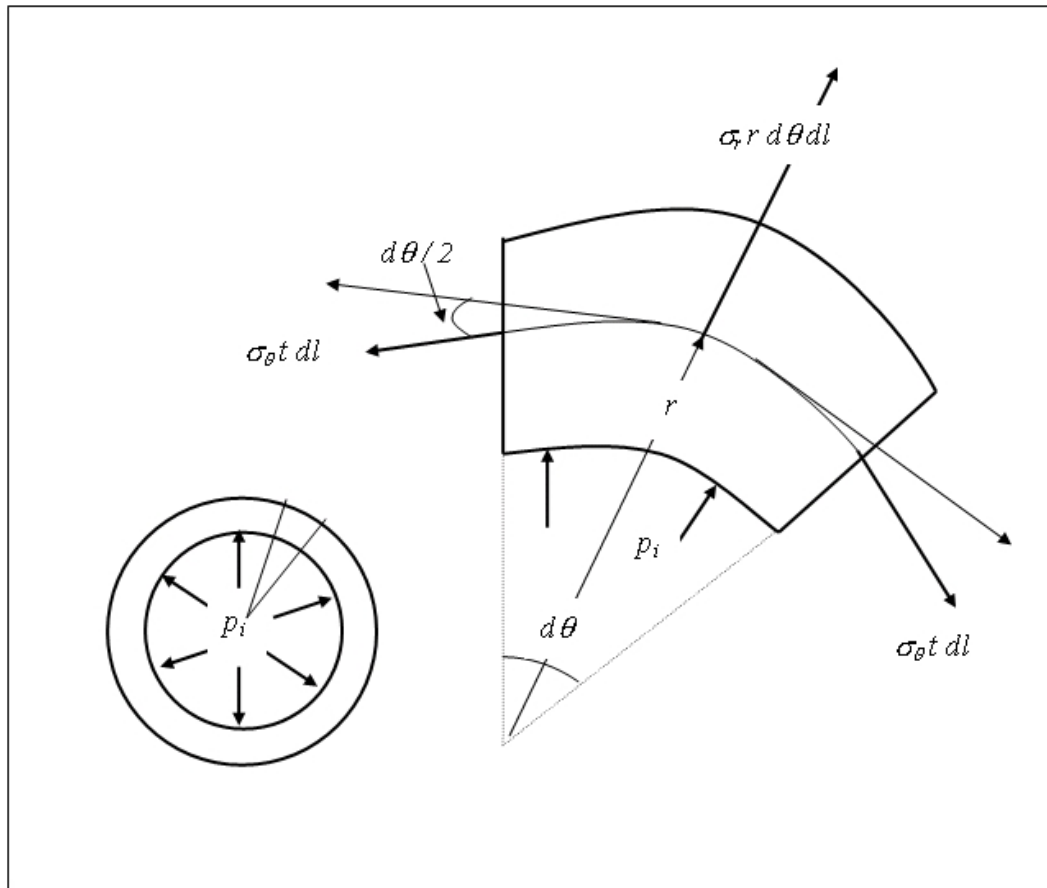
Figure 4-2: Force Balance Analysis - Radial Direction

Balancing the forces along the radial direction from Fig. 4-2,

$$p_i r d\theta dl + \sigma_r r d\theta dl = 2\sigma_\theta \sin\left(\frac{d\theta}{2}\right) t dl \qquad (4\text{-}8)$$

$\sin\left(\dfrac{d\theta}{2}\right)$ is small $\approx \left(\dfrac{d\theta}{2}\right)$

where, p_i is the internal pressure

r is the mean radius

dl is length of element in z direction

$d\theta$ is the small angle in hoop direction

Therefore, equation (4-8) becomes,

$$p_i r d\theta dl + \sigma_r r d\theta dl = 2\sigma_\theta \left(\frac{d\theta}{2} \right) t dl \qquad (4\text{-}9)$$

$$p_i \frac{r}{t} + \sigma_r \frac{r}{t} = \sigma_\theta \qquad (4\text{-}10)$$

4.2.1   Internal Pressure (THF)

With only internal pressure,

$$\sigma_r = 0 \qquad (4\text{-}11)$$

and, equation (4-10) becomes,

$$\sigma_\theta = \frac{p_i r}{t} \qquad (4\text{-}12)$$

Plane strain condition will be considered wherein $\varepsilon_z = 0$, the volume constancy would give $\varepsilon_t = -\varepsilon_\theta$. The deviatoric stress, $\sigma_z{}' = 0$.

The normal axial stress,

$$\sigma_z = \frac{1}{2}\sigma_\theta \qquad (4\text{-}13)$$

Mellor used an argument of 'incipient bulging' similar to 'incipient necking' in the simple tension test to establish the instability criterion for thin walled tubes with only internal pressure [22]. The results obtained by Mellor are outlined below [22]:

$$\frac{1}{\bar{\sigma}}\frac{d\bar{\sigma}}{d\bar{\varepsilon}} = \frac{1}{z} = \sqrt{3} \quad \text{where, z is the sub-tangent modulus} \tag{4-14}$$

and the critical effective strain is,

$$\bar{\varepsilon}^* = nz = n\frac{1}{\sqrt{3}} = \frac{n}{\sqrt{3}} \tag{4-15}$$

4.2.2 Internal Pressure and Independent Axial Load (THF)

Mellor, while establishing the instability criterion for combined loading in thin walled tubes emphasized the importance of generalized stress and strain [22]. He pointed out that the results of plastic instability should not be only in terms of maximum principal strains because that method obscures the relative ductility of a particular material under different stress systems. In the analysis of plastic instability for thin-walled tubes under internal pressure and independent axial loading, the loads for this case were assumed to be applied in such a manner that the ratio of longitudinal to hoop stress remains constant so as to have a simple theoretical analysis [22].

A similar approach to that outlined above was used by Mellor to establish a plastic instability criterion for local bulging with internal pressure and independent axial load to obtain the following results [22].

Sub-tangent modulus, $z = \dfrac{2}{3}\left[\left(\dfrac{\sigma_z}{\sigma_\theta}\right)^2 - \left(\dfrac{\sigma_z}{\sigma_\theta}\right) + 1\right]^{1/2}$ (4-16)

Critical strain, $\bar{\varepsilon}^* = nz = \dfrac{2}{3}\left[\left(\dfrac{\sigma_z}{\sigma_\theta}\right)^2 - \left(\dfrac{\sigma_z}{\sigma_\theta}\right) + 1\right]^{1/2} n$ (4-17)

The instability criterion can be obtained from equations (4-17) and (4-18) for different ratios of axial stress to hoop stress.

4.2.3   Internal Pressure and Counter Pressure (DHF)

With internal pressure and external pressure of p_o,

$$\sigma_r \approx -p_o$$ (4-18)

Therefore, equation (4-10) becomes,

$$\sigma_\theta = (p_i - p_o)\dfrac{r}{t}$$ (4-19)

A plane strain condition will be considered wherein $\varepsilon_z = 0$, the volume constancy would give $\varepsilon_t = -\varepsilon_\theta$. The deviatoric stress, $\sigma_z' = 0$.

The normal axial stress,

$$\sigma_z = \dfrac{1}{2}(\sigma_\theta + \sigma_r)$$ (4-20)

Let a small increment $\delta\bar{\varepsilon}$ be imposed when the stress is $\bar{\sigma}$.

Work hardening requires that the internal pressure be increased by an amount

$$\frac{t}{r}\frac{2}{\sqrt{3}}\frac{d\bar{\sigma}}{d\bar{\varepsilon}}\delta\bar{\varepsilon} \tag{4-21}$$

The change in geometry corresponds to a reduction in pressure of

$$-\sqrt{3}\frac{t}{r}\left(\frac{2}{\sqrt{3}}\bar{\sigma}-p_o\right)\delta\bar{\varepsilon} \tag{4-22}$$

Using an argument of 'incipient bulging' similar to incipient necking in the simple tension test, the process will become unstable when the increase in internal pressure due to work hardening is balanced by the reduction in pressure due to geometry changes.

That is, equation (4-21) + equation (4-22) = 0

$$\frac{t}{r}\frac{2}{\sqrt{3}}\frac{d\bar{\sigma}}{d\bar{\varepsilon}}\delta\bar{\varepsilon}+\left[-\sqrt{3}\frac{t}{r}\left(\frac{2}{\sqrt{3}}\bar{\sigma}-p_o\right)\delta\bar{\varepsilon}\right]=0 \tag{4-23}$$

Dividing equation (4-23) by $\dfrac{2\bar{\sigma}}{\sqrt{3}}\dfrac{t}{r}$ and rearranging, we get

$$\frac{1}{\bar{\sigma}}\frac{d\bar{\sigma}}{d\bar{\varepsilon}}=\sqrt{3}\left(1-\frac{\sqrt{3}}{2}\frac{p_o}{\bar{\sigma}}\right)=\frac{1}{z} \quad \text{where, z is the sub-tangent modulus.} \tag{4-24}$$

Therefore, $z = \dfrac{1}{\left(1 - \dfrac{\sqrt{3}p_o}{2\bar{\sigma}}\right)\sqrt{3}}$ (4-25)

Hence, critical effective strain,

$$\bar{\varepsilon}^* = nz = \dfrac{n}{\left(1 - \dfrac{\sqrt{3}p_o}{2\bar{\sigma}}\right)\sqrt{3}}$$ (4-26)

4.2.4 Internal Pressure, Independent Axial Load and External Pressure (DHF)

With internal pressure and external pressure of p_o,

$$\sigma_r \approx -p_o$$ (4-27)

Therefore, equation (4-10) changes to,

$$\sigma_\theta = (p_i - p_O)\dfrac{r}{t}$$ (4-28)

The analysis of the instability for a thin-walled tube under internal pressure, external pressure and independent axial loading, assumes the ratio of longitudinal to hoop stress remains constant and also the ratio of external pressure to hoop stress remains constant.

In local bulging, let a small increment $\delta\bar{\varepsilon}$ be imposed when the stress is $\bar{\sigma}$.

Work hardening requires that the internal pressure be increased by an amount,

$$\frac{t}{r}\frac{1}{\lambda}\frac{d\overline{\sigma}}{d\overline{\varepsilon}}\delta\overline{\varepsilon} \tag{4-29}$$

The change in geometry corresponds to a reduction in pressure of

$$\frac{-3}{2}\frac{\overline{\sigma}}{\lambda}\frac{\sigma_\theta}{\overline{\sigma}}\frac{t}{r}\delta\overline{\varepsilon} \tag{4-30}$$

Using an argument of 'incipient bulging' similar to incipient necking in the simple tension test the process will become unstable when the increase in internal pressure due to work hardening is balanced by the reduction in pressure due to geometry changes.

That is, instability occurs when,

Equation (4-29) + Equation (4-30) = 0

$$\frac{t}{r}\frac{1}{\lambda}\frac{d\overline{\sigma}}{d\overline{\varepsilon}}\delta\overline{\varepsilon} + \left[\frac{-3}{2}\frac{\overline{\sigma}}{\lambda}\frac{\sigma_\theta}{\overline{\sigma}}\frac{t}{r}\delta\overline{\varepsilon}\right] = 0 \tag{4-31}$$

Solving equation (4-31),

$$\frac{1}{\overline{\sigma}}\frac{d\overline{\sigma}}{d\overline{\varepsilon}} = \frac{3}{2}\frac{1}{\lambda} = \frac{1}{z} \quad \text{where, z is the sub-tangent modulus} \tag{4-32}$$

$$z = \frac{2}{3}\lambda = \frac{2}{3}\left[1+\left(\frac{\sigma_z}{\sigma_\theta}\right)^2+\left(\frac{p_o}{\sigma_\theta}\right)^2+\left(\frac{\sigma_z}{\sigma_\theta}\frac{p_o}{\sigma_\theta}\right)-\left(\frac{\sigma_z}{\sigma_\theta}\right)+\frac{p_o}{\sigma_\theta}\right]^{\frac{1}{2}} \tag{4-33}$$

Hence, critical strain,

$$\overline{\varepsilon}^* = nz = \frac{2}{3}\left[1 + \left(\frac{\sigma_z}{\sigma_\theta}\right)^2 + \left(\frac{p_o}{\sigma_\theta}\right)^2 + \left(\frac{\sigma_z}{\sigma_\theta}\frac{p_o}{\sigma_\theta}\right) - \left(\frac{\sigma_z}{\sigma_\theta}\right) + \frac{p_o}{\sigma_\theta}\right]^{1/2} n \qquad (4\text{-}34)$$

4.2.5 Results and Discussion

Table 4-1 lists instability criterion for tube hydroforming (internal pressure only and internal pressure + axial load) and dual hydroforming (internal pressure + counter pressure and internal pressure + axial load + counter pressure).

Table 4-1: Instability Criterion: Critical Strain

Loading Conditions	Plastic Instability Critical strain = nz
Internal Pressure	$\dfrac{n}{\sqrt{3}}$
Internal Pressure + Axial Load	$\dfrac{2}{3}\left[\left(\dfrac{\sigma_z}{\sigma_\theta}\right)^2 - \left(\dfrac{\sigma_z}{\sigma_\theta}\right) + 1\right]^{1/2} n$
Internal Pressure + Counter Pressure	$\dfrac{n}{\left(1 - \dfrac{\sqrt{3}p_o}{2\sigma}\right)\sqrt{3}}$
Internal Pressure + Axial Load+ Counter Pressure	$\dfrac{2}{3}\left[1 + \left(\dfrac{\sigma_z}{\sigma_\theta}\right)^2 + \left(\dfrac{p_o}{\sigma_\theta}\right)^2 + \left(\dfrac{\sigma_z}{\sigma_\theta}\dfrac{p_o}{\sigma_\theta}\right) - \left(\dfrac{\sigma_z}{\sigma_\theta}\right) + \dfrac{p_o}{\sigma_\theta}\right]^{1/2} n$

From the instability theory, it is found that the ductility of metal is an inherent property of material and is also subjected to modification by the imposed stress system. The instability strain for a thin walled tube with only internal pressure is less than that of uniaxial tensile test ($n/\sqrt{3} < n$). With combined loading of internal and external pressure, the critical instability strain increases

$$\frac{n}{\sqrt{3}\left(1 - \sqrt{3}\,p_o\Big/2\bar{\sigma}\right)} \geq \frac{n}{\sqrt{3}}.$$

As p_0 increases, the denominator becomes smaller and the effective strain to failure becomes larger. With no counter pressure ($p_o = 0$), the instability criterion reduces to that of tube with only internal pressure. The benefit of applying counter pressure is thus demonstrated.

With axial feeding, the instability criterion,

$$\frac{2}{3}\left[\left(\frac{\sigma_z}{\sigma_\theta}\right)^2 - \left(\frac{\sigma_z}{\sigma_\theta}\right) + 1\right]^{1/2} n > \frac{n}{\sqrt{3}}$$

Axial loading assists in delaying the onset of plastic instability. This supports the application of axial feeding in industrial THF process. The instability criterion for combined loading of internal pressure, axial load and counter pressure is given by

$$\frac{2}{3}\left[1 + \left(\frac{\sigma_z}{\sigma_\theta}\right)^2 + \left(\frac{p_o}{\sigma_\theta}\right)^2 + \left(\frac{\sigma_z}{\sigma_\theta}\frac{p_o}{\sigma_\theta}\right) - \left(\frac{\sigma_z}{\sigma_\theta}\right) + \frac{p_o}{\sigma_\theta}\right]^{1/2} n.$$

Without axial load for $\sigma_z = \dfrac{1}{2}(\sigma_\theta + \sigma_r)$, the equation reduces to that of the thin walled-

tube subjected to internal pressure and external pressure i.e. $\dfrac{n}{\left(1 - \sqrt{3}p_o \middle/ 2\bar{\sigma}\right)\sqrt{3}}$

(Appendix E for details).

This leads to the conclusion that,

$$\frac{2}{3}\left[1 + \left(\frac{\sigma_z}{\sigma_\theta}\right)^2 + \left(\frac{p_o}{\sigma_\theta}\right)^2 + \left(\frac{\sigma_z}{\sigma_\theta}\frac{p_o}{\sigma_\theta}\right) - \left(\frac{\sigma_z}{\sigma_\theta}\right) + \frac{p_o}{\sigma_\theta}\right]^{\frac{1}{2}} n > \frac{n}{\sqrt{3}\left(1 - \sqrt{3}p_o \middle/ 2\bar{\sigma}\right)}.$$

That is, in the presence of both internal and external pressure, axial feed will increase the critical instability strain.

With no counter pressure ($p_o = 0$), instability criterion (4-34) reduces to (4-17) the same as that for combined loading of internal pressure and axial loading. As p_o increases, the effective strain to failure also increases as,

$$\frac{2}{3}\left[1 + \left(\frac{\sigma_z}{\sigma_\theta}\right)^2 + \left(\frac{p_o}{\sigma_\theta}\right)^2 + \left(\frac{\sigma_z}{\sigma_\theta}\frac{p_o}{\sigma_\theta}\right) - \left(\frac{\sigma_z}{\sigma_\theta}\right) + \frac{p_o}{\sigma_\theta}\right]^{\frac{1}{2}} n > \frac{2}{3}\left[\left(\frac{\sigma_z}{\sigma_\theta}\right)^2 - \left(\frac{\sigma_z}{\sigma_\theta}\right) + 1\right]^{\frac{1}{2}} n$$

The potential of using dual pressure to improve the THF process is again demonstrated. The effect of applying counter pressure to tube hydroforming in terms of plastic instability is illustrated by considering a tube with mean radius (r) of 12.06 mm and

thickness (*t*) of 1.37 mm. A hardening exponent (*n*) of 0.35 (for copper), an internal pressure (p_i) of 40 MPa and a counter pressure (p_o) of 7 MPa are taken into account. Table 4-2 illustrates the difference in effective strain for internal pressure only and a combination of internal and external pressure.

Table 4-2: Effective Strain to Failure

Loading Condition	Critical Strain
Internal pressure	0.2021
Internal + Counter pressure	0.2069

When using both internal pressure and counter pressure (DHF), the tube can be deformed to a higher level of effective strain before fracture as compared to only internal pressure (THF). Thus, the addition of counter pressure results in a better material shaping capability by delaying the onset of plastic instability.

Comparison for the two cases - a) Internal Pressure + Axial Load and b) Internal Pressure + Axial Load + Counter Pressure can be drawn by considering various ratios of hoop to axial stress as shown in Fig 4-3.
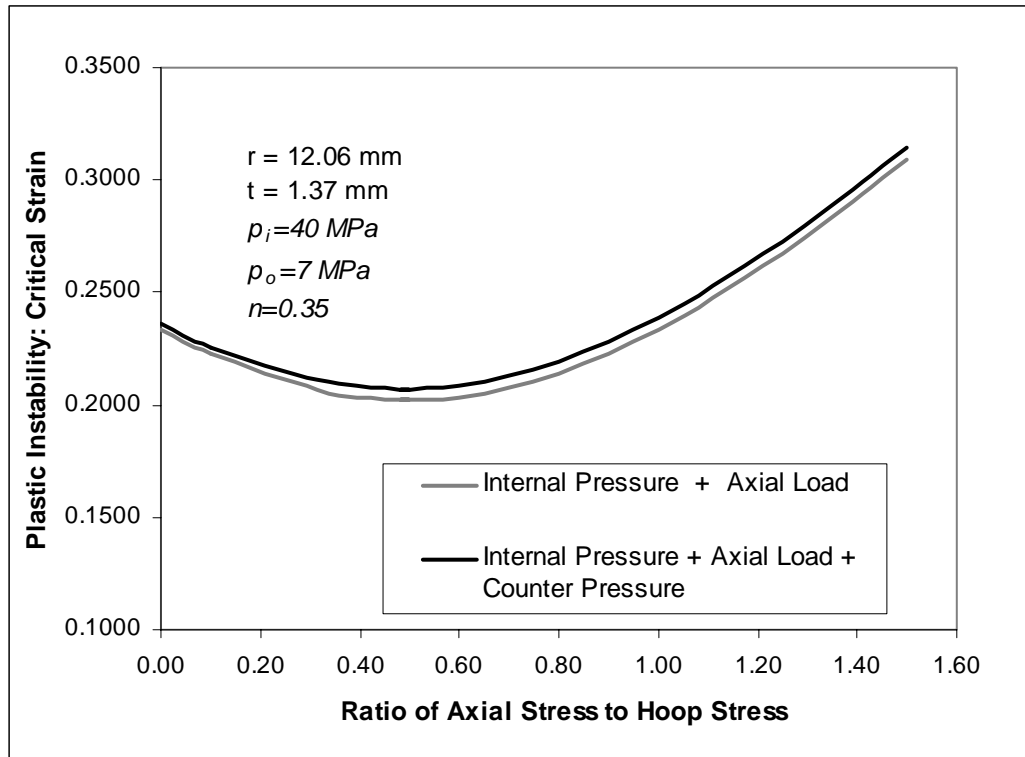
Figure 4-3: Effective Strain: Tube Hydroforming and Dual Hydroforming

In dual hydroforming for a given ratio of hoop to axial stress, better final bulged configuration can be achieved compared to tube hydroforming as the addition of counter pressure increases the value of effective strain to failure.

4.3 Finite Element Analysis – Plastic Instability

The analytical model developed considered proportional loading, i.e., ratio of axial to hoop stress remains constant. In the simulation it was difficult to prescribe such a

loading condition; hence, a linear loading path is followed for internal pressure, axial feed and counter pressure.

The internal hydraulic pressure of 40 MPa was applied as a uniformly distributed load to the tube inner surface and was introduced as a linearly increasing function of time. The axial stroke of 12 mm was applied as a prescribed displacement of the punch at the edge of the tube, also as a linearly increasing function of time. The external counter pressure of 7 MPa was also applied as a linearly increasing function of time.

Two different loading conditions were analyzed. The initial run was without applying external counter pressure as Load Pattern 1 shown in Fig. 4-4 (THF). Keeping the same internal pressure and axial feed curves, the analysis followed with external counter pressure as Load Pattern 2 shown in Fig. 4-5 (DHF).
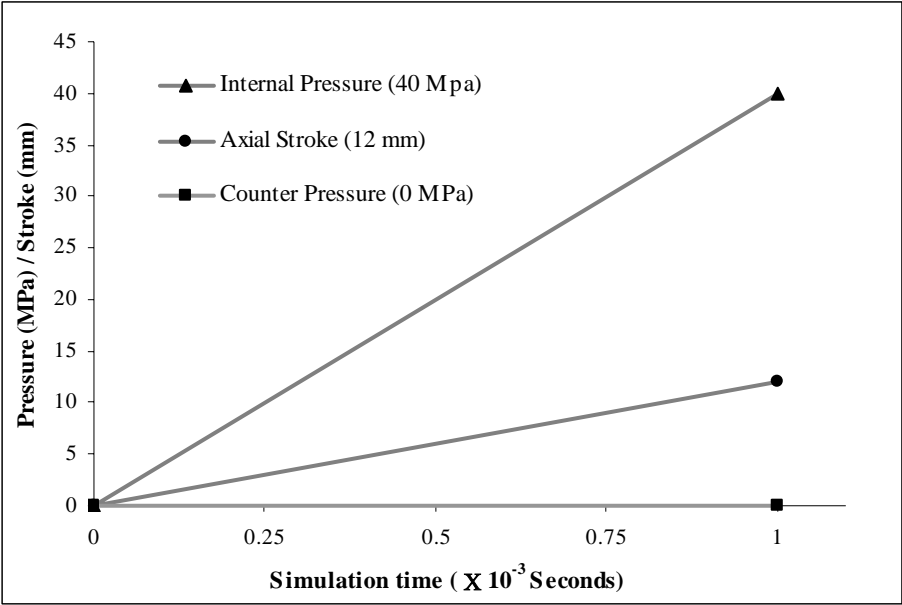
Figure 4-4: Load Pattern 1 – THF
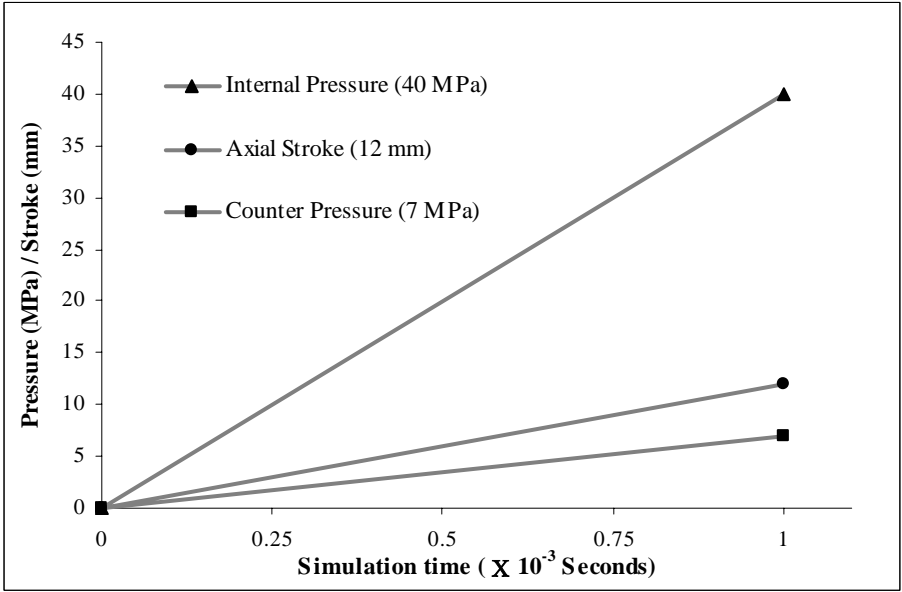
Figure 4-5: Load Pattern 2 – DHF

The ratio of axial to hoop stress $\dfrac{\sigma_z}{\sigma_\theta}$ is taken from the finite element simulation as 0.2203

and $\dfrac{p_0}{\sigma_\theta} = 0.0240$. The strain hardening exponent is assumed to be 0.35.

The tube properties as used earlier in this section are used to illustrate the effect of counter pressure on the final bulged configuration using plastic instability criterion.

Tube Hydroforming (without external pressure)

$$\overline{\varepsilon} = \frac{2}{3}\left[\left(\frac{\sigma_z}{\sigma_\theta}\right)^2 - \left(\frac{\sigma_z}{\sigma_\theta}\right) + 1\right]^{\frac{1}{2}} \quad n = 0.2124$$

Dual Hydroforming (with external pressure)

$$\overline{\varepsilon} = \frac{2}{3}\left[1 + \left(\frac{\sigma_z}{\sigma_\theta}\right)^2 + \left(\frac{p_o}{\sigma_\theta}\right)^2 + \left(\frac{\sigma_z}{\sigma_\theta}\frac{p_o}{\sigma_\theta}\right) - \left(\frac{\sigma_z}{\sigma_\theta}\right) + \frac{p_o}{\sigma_\theta}\right]^{\frac{1}{2}} \quad n = 0.2162$$

The bulge height for tube hydroforming and dual hydroforming for effective strain of 0.2124 and 0.2162 were compared respectively and tabulated in Table 4-3.

Table 4-3: Effective Strain and Bulge Height for THF and DHF

	Effective Strain	Bulge Height (mm)
Tube Hydroforming	0.2124	6.07
Dual Hydroforming	0.2162	6.62

In dual hydroforming there is an increase of 8.03 % in bulge height for a value of counter pressure that is only 17.5 % of internal pressure. Hence, a better final bulged configuration can be obtained with dual hydroforming.

CHAPTER V

INFLUENCE OF MATERIAL PROPERTIES

The tube material properties, such as yield strength, anisotropic values, hardening exponent and process condition such as friction, affect the tube deformation process. Simulations of cross joints bulge forming have been carried out for different material properties, such as anisotropic values, strain hardening parameters, and different coefficients of friction as listed in Table 5-1.

Table 5-1: Different Anisotropic Values, Strain Hardening Parameters, and Coefficients of Friction

Parameters			
Anisotropic value, r	0.6	1.0	1.6
Strain hardening exponent, n	0.2	0.3	0.4
Coefficient of friction, μ	0.04	0.10	0.20

The values for process parameters have been chosen keeping in mind the practical and industrial standpoint. In copper, anisotropy value, r, ranges from 0.6 to 0.9 [2]. The strain hardening exponent (n) ranges from 0.35 to 0.5 for copper and is around 0.2 for aluminum [2]. In many applications in industry, the fluid, which is used to generate internal pressure, acts as lubricant. This fluid is a mix of oil and water (emulsion) and results in a coefficient of friction in the range of 0.15 - 0.20. Dry lubricants are rarely used in the tube hydroforming process. The value of coefficient of friction for dry lubricants is in the range of 0.04 to 0.06.

For a certain parameter, the initial run is without applying external counter pressure as Load Pattern 1 shown in Fig. 5-1. The minimum thickness on the tube is recorded with increasing bulge height. Keeping the same internal pressure and axial feed curves, the external pressure (12.5 % of internal pressure) is applied as a linearly increasing function (Load Pattern 2) as shown in Fig. 5-2. Once again the minimum thickness is recorded with increasing bulge height.

To characterize dual hydroforming processes based upon different process parameters, the *increase in minimum thickness* resulting from Load Pattern 1 and Load Pattern 2 is plotted for different parameters against increasing bulge height and compared.
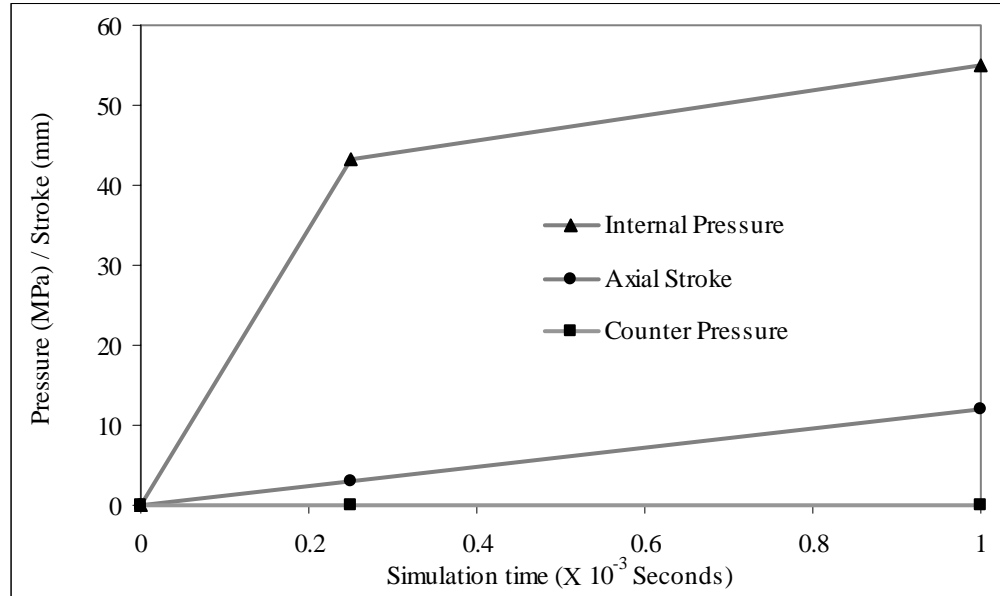
Figure 5-1: Variation of Pressure and Stroke with Time for Load Pattern 1
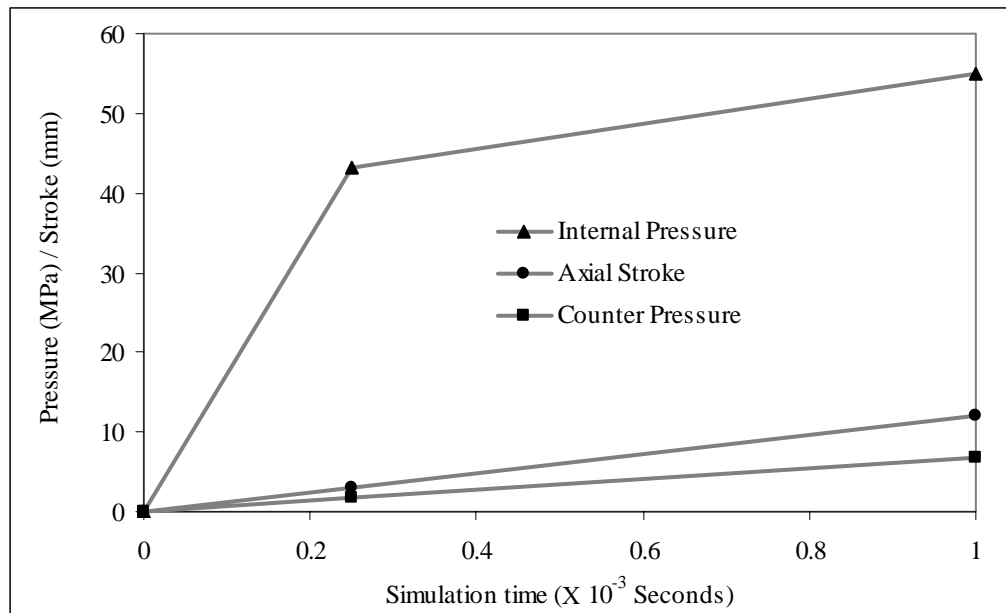
Figure 5-2: Variation of Pressure and Stroke with Time for Load Pattern 2

5.1 Effect of Strain Hardening Exponent, *n*

Different strain hardening exponent values, as listed in Table 5-1, were compared. Strain

hardening is the most crucial factor affecting formability. It is advisable to use a high *n*

value sheet for processes involving biaxial stretching [57].

Asnafi, using free bulging tube deformation showed that equivalent strain to plastic instability can be written as [58]:

$$\varepsilon_f = (1 + r) \cdot n \qquad (5\text{-}1)$$

where r = anisotropy value

n = strain hardening exponent

The above equation indicates that the higher the n value the more formability there is for a given r value. As outlined in various papers, [16, 18], the effect of n is not significant for wall thickness distribution and the attainable bulge height for tube hydroforming process. Also, Carleer et al. [28] summarized that n values have hardly any influence on the strain distribution in the forming diagram and the strain path for all n values in the forming limit diagram remains unchanged.

The increase in minimum thickness is 0.018 mm for $n = 0.40$ as compared to an increase in minimum thickness of 0.014 mm for $n = 0.20$ (Fig. 5-3). The difference is quite small and suggests that n values have the slightest of effect in the dual tube hydroforming process. This seems plausible as tube hydroforming forms the basis for dual hydroforming. The strain hardening parameter (n) has the least effect on strain distribution in tube hydroforming.
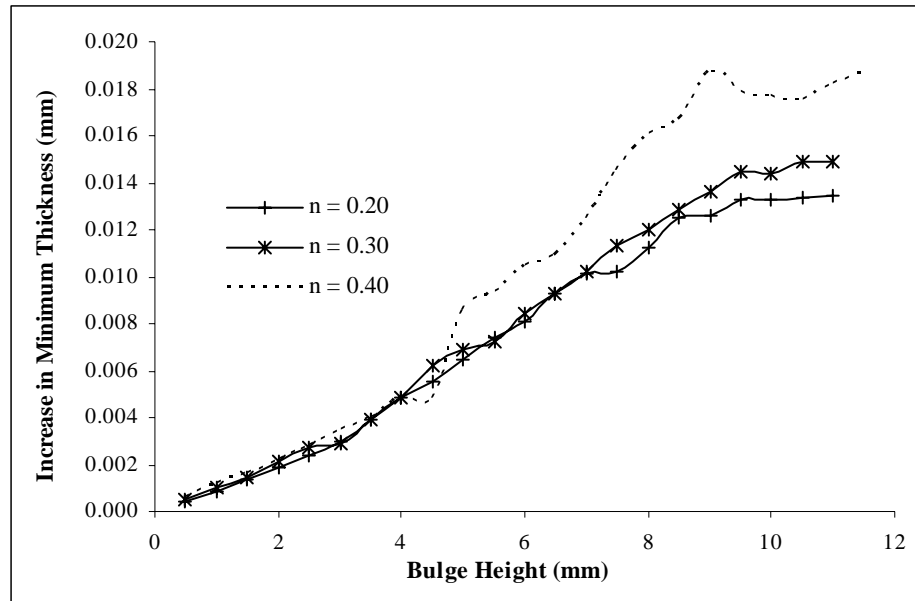
Figure 5-3: Effect of Strain Hardening Parameter on DHF

5.2 Effect of Anisotropy, *r*

A lower *r* value indicates easy thinning and a larger *r* value indicates resistance to thinning. Material flow depends considerably on anisotropic values and thus it becomes a crucial parameter. Many materials, such as aluminum alloys and copper, which are widely used, have anisotropic values less than 1. As outlined in the analytical model developed by Ansafi [58], the fracture strain for a tube produced by bending and welding of rectangular sheets, is

$$\varepsilon_{if} = \frac{(1+r)n - \sqrt{\frac{4}{3}\ln\left(1+\frac{t_o}{d_0}\right)}}{\left[\frac{4}{3}\left(1+\beta+\beta^2\right)\right]^{1/2}} \tag{5-2}$$

The fracture strain for extruded profiles is:

$$\varepsilon_{1f} = \frac{(1+r)n}{\left[\frac{4}{3}\left(1 + \beta + \beta^2\right)\right]^{1/2}}$$

(5-3)

where, ε_{if} = major strain at fracture

r = anisotropy value

n = strain hardening exponent

$\beta = \varepsilon_2/\varepsilon_1$; ε_1 is hoop strain and ε_2 is tangential strain

The above equations indicate that the formability reduces with reduced r value, other parameters being constant. Dual hydroforming, thus, should become rewarding for materials with lesser anisotropic values which are less formable. Figure 5-4 shows that for lower r values, which result in more thickness variation, the dual hydroforming process is more productive. The increase in minimum thickness is around 0.05 mm for r = 0.6 compared to 0.01 mm for r = 1.6.
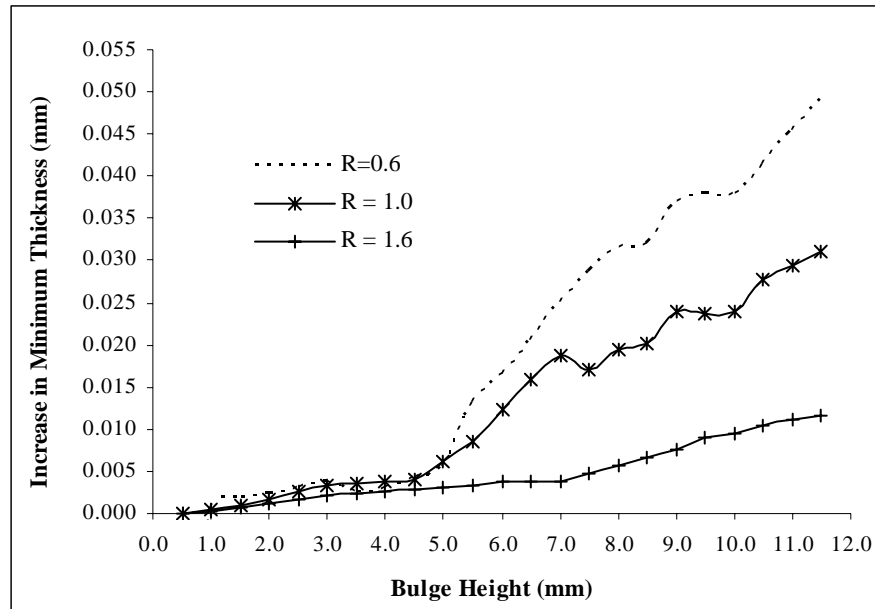
Figure 5-4: Effect of Anisotropic Value on Dual Hydroforming Process

5.3 Effect of Friction

It is known that the amount of friction acting between the tube blank and the die establishes the level of deformation. Friction limits the extent of bulge forming process, since the material cannot flow easily. The resistance offered by friction increases with internal pressure as it pushes the tube against the surfaces of the die. Friction also plays an important role when axial feeding is applied to avoid thinning. As explained by Duncan et al., the effect of this axial feeding is local since friction between the die wall and tube will cause it to weaken with distance from the point of the application of force. The equation for axial or hoop tension is listed below [57]

$$dT_{\phi} = \mu q dz \tag{5-4}$$

where q = contact pressure between die and tube,

T_φ = axial or hoop tension, and

dz = small increment of distance in axial direction

which shows that compression decreases with increased distance from the end of the tube. The larger the value of the coefficient of friction, the smaller is the effect of axial feeding. Hence, larger values of coefficient of friction result in more thinning.

As shown in Fig. 5-5, at the end of simulation time, the large value of coefficient of friction resulted in a lesser bulge height, showing the effect of axial feeding becoming lesser for higher values, as a result of less material flow taking place. The dual hydroforming process becomes more effective for higher values of coefficient of friction. The curve shifts upwards as the coefficient of friction increases. For a bulge height of 11.00 mm, the increase in minimum thickness is 0.034 mm for $\mu = 0.20$ and the increase in minimum thickness is 0.028 mm for $\mu = 0.04$. In industry, for many applications, fluid (hydraulic oil) used as the pressurizing medium acts as lubricant. It has a coefficient of friction around 0.15 to 0.20 which is large compared to a coefficient of friction due to the use of lubricants. Thus, the effect of dual hydroforming will be significant in industrial settings.
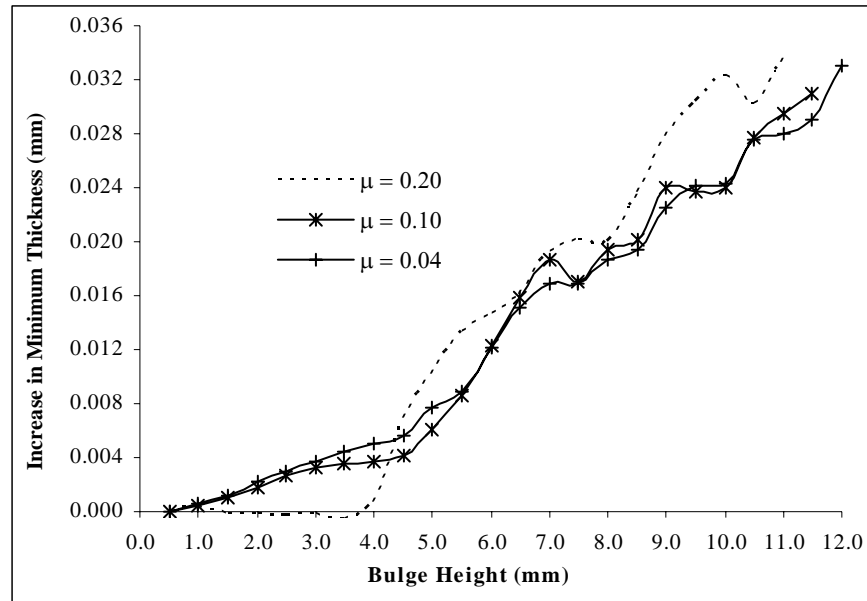
Figure 5-5: Effect of Friction on Dual Hydroforming Process

5.4 Effect of Material: Aluminum, Copper and Steel

The study has been extended to compare different materials including aluminum alloy, copper and steel. The material properties as listed in Table 5-2 have been taken from various references [30, 60].

Table 5-2: Material Properties for Aluminum Alloy, Copper and Steel

Material Properties for Aluminum, Copper and Steel			
	Aluminum	Steel	Copper
Young's modulus (MPa)	70×10^3	210×10^3	124×10^3
Yield strength (MPa)	180	430	160
K (MPa)	533.13	938.25	618.30
n	0.2837	0.2376	0.4000
Poisson's ratio	0.33	0.33	0.30
Density (kg/mm^3)	2.7×10^{-6}	7.9×10^{-6}	8.9×10^{-6}

The simulations for dual hydroforming have been carried out with material properties of aluminum alloy, copper and steel. The material model *MAT_PIECEWISE_LINEAR_ PLASTICITY takes into account elastic modulus, yield strength and tangent modulus. The strength coefficient K, strain hardening exponent n, and yield strength as listed in Table 5-2 are used to obtain tangent modulus as required by the material model. The steel has good formability and higher strength as compared to copper and aluminum alloy. In general aluminum alloys have low r value and are more prone to thinning. Copper strain hardens easily having strain hardening exponents, n, ranging from 0.35 to 0.5 and also the normal anisotropy value is low ($r = 0.6$ to 0.9) [2]. For the simulations, anisotropy is not considered and the same coefficient of friction is used. The tube for different materials was subjected to different internal pressure (40 MPa for Aluminum, 55 MPa for Copper and 80 MPa for steel) but same axial feeding so as to obtain nearly the same bulge height. The counter pressure was 12.5% of the internal pressure applied. Figure 5-6 shows that greater improvement in terms of thickness can be achieved for copper and aluminum as compared to steel for a bulge height of 12 mm. However, improvements in minimum thickness due to counter pressure were observed for all materials.
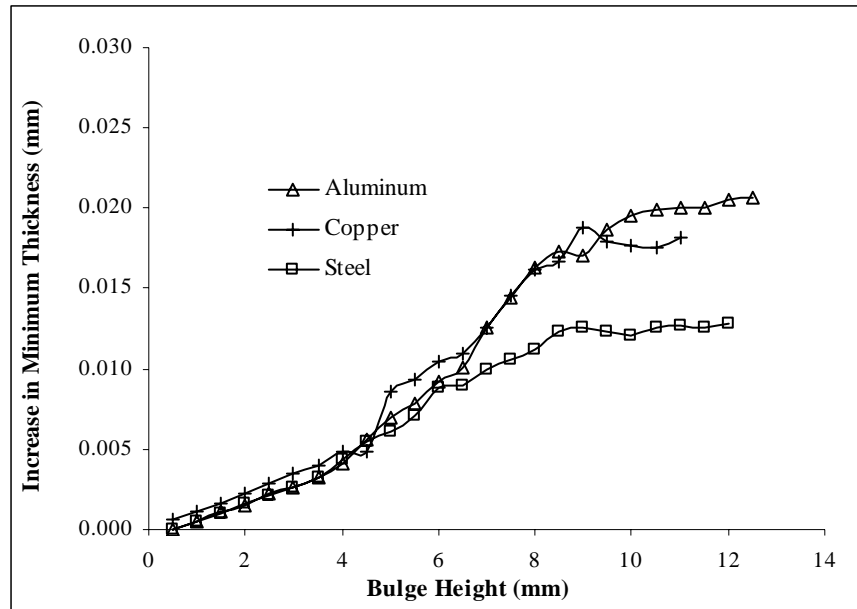
Figure 5-6: Effect of Different Materials on Dual Hydroforming Process

CHAPTER VI

CONCLUSIONS

The new process parameter, counter-pressure, introduced in the conventional tube hydroforming process resulted in a favorable tri-axial stress state during the deformation process. The stress state at a given time and location varies with the process history, design and control of the load paths. The counter pressure provided back support to the tube material and dual hydroforming resulted in less thinning. With the use of the dual pressure system and end feeding, better final bulged configuration can be achieved.

Ductility and formability of the material can be influenced by the stress system. The addition of counter pressure resulted in delayed onset of plastic instability, that is, the material can be strained to a higher value of effective strain. Also, as counter pressure increases, the value of effective strain to failure increases. For $p_o = 0$, the instability criterion for a thin walled tube with counter pressure is reduced to the same instability criterion for a thin walled tube without counter pressure. Dual hydroforming provides improved material handling capabilities due to larger failure strain, which will result in enhanced final configuration.

The effects of material properties and friction were investigated. In the conventional tube hydroforming process, the crucial parameters for strain distribution are anisotropy value and coefficient of friction. These parameters also have a major effect on the dual

hydroforming process as verified by simulations. While resulting in a more even strain distribution, the dual tube hydroforming process becomes meritorious in low anisotropy and/or high friction conditions.

The process can be introduced to achieve larger expansion and more complex deformation geometry. Also, converting to a higher strength and less formable materials becomes possible.

As part of future work, optimization of loading paths can be considered to obtain a superior final bulged configuration. An analytical model could be developed to demonstrate the effect of counter pressure on wrinkling. This work only establishes the merit of applying counter pressure. Work has to be done in the area of die and tooling design and implementation of counter pressure in industry.

REFERENCES

1. Koc M., and Altan T., 2001, "An overall review of the tube hydroforming (THF) technology," Journal of Materials Processing and Technology, **108** (3), pp. 384-393.

2. Hosford W.F., and Caddell, R.M., 1983, *Metal Forming Mechanics and Metallurgy*, Prentice Hall, Inc., Englewood Cliffs, NJ.

3. Hoffmanner A.L., 1967 "Correlation of Fracture Strain with Ratio of Hydrostatic Stress to Effective Stress," Interim report, Air Force Contract F 33615-67-C-1466, TRW.

4. Rogersand H.C., and Coffin L.F., Jr., 1967, Final Report, Contract No-66-0546-d, Naval Air Systems Command.

5. Cockcroft M.G., and Latham D.J., 1968, "Ductility and the workability of metals," Journal of Institute of Metals, **96,** pp. 33-39.

6. Atkins A. G., 1981, "Possible explanation for unexpected departures in hydrostatic tension – fracture strain relations," Metal Science, Feb. 1981, pp. 81-83.

7. Ghosh A.K., 1976, "Criterion for ductile fracture in sheets under biaxial loading," Metallurgical Transactions A - Physical Metallurgy and Materials Science, **7**, pp. 523-533.

8. McClintock F.A. J., 1968 , "A criterion for ductile fracture by the growth of holes," Journal of Applied Mechanics, Transaction ASME, **35**, pp. 363-371.

9. Finckenstein, E., Kleiner, M., Homberg, W., and Szucs, E., 1998, "In-process punching with pressure fluids in sheet metal forming," Annals of the CIRP, **47**, pp. 207-212.

10. Thiruvarudchel, van S., and Wang, H., 1998, "Hydraulic pressure enhancement of the deep drawing process to yield deeper cups," Journal of Materials Processing Technology, **82**, pp. 156-164.

11. Altan, T., 1999, "R&D update – sheet hydroforming," Stamping Journal, November/December, pp. 90-93.

12. Hein, P. and Vollertsen, F., 1999 "Hydroforming of sheet metal pairs," Journal of Materials Processing Technology, **87** (1-3), pp. 154-164.

13. Liu, J., Atmetoglu, M., and Altan, T, 2000, "Evaluation of sheet metal formability, viscous pressure forming (VPF) dome test," Journal of Material Processing Technology, **98**, pp. 1-6.

14. Lo, S.-W., Hsu, T.-Z., and Wilson, W. R. D., 1993, "An analysis of the hemispherical-punch hydroforming processes," Journal of Material Processing Technology, **37**, pp. 225-239.

15. Yossifon S., Tirosh J., and Kochavi E., 1984, "On suppression of plastic buckling in hydroforming processes," International Journal of Mechanical Science, **26** (6-8), pp. 389-402.

16. Yossifon, S. and Tirosh, J., 1985, "Rupture instability in hydroforming deep-drawing process," International Journal of Mechanical Science, **27** (9), pp. 559-570.

17. Ahmed M., and Hashmi M.S.J., 1997, "Comparison of free and restrained bulge forming by finite element method simulation," Journal of Materials Processing Technology, **63**, pp. 651-654.

18. Nakagawa T., Nakamura K., and Amino H., 1997, "Various applications of hydraulic counter-pressure deep drawing," Journal of Materials Processing Technology, **71**, pp. 160-167.

19. Amino H., Nakamura K., and Nakagawa T., 1990, "Counter-pressure deep drawing and its application in the forming of automobile parts," Journal of Materials Processing Technology, **23**, pp. 243-265.

20. Koc M., and Altan T., 2002, "Prediction of forming limits and parameters in the tube hydroforming process," International Journal of Machine Tools & Manufacture, **42**, pp. 123-138.

21. Tonghai W., Sheng S., and Dexiu M., 1993, "The research of tube bulging using polyurethane under compound external forces and its application," Advanced Technology Plasticity, **1,** pp. 494-499.

22. Mellor P. B., 1962, "Tensile instability in thin-walled tubes," Journal of Mechanical Engineering Science, **4**, pp. 251-256.

23. Hillier M.J., 1963, "Tensile plastic instability under complex stress," International Journal of Mechanical Science, **5**, pp. 57-67.

24. Hillier M.J., 1965, "Tensile plastic instability of thin tubes - I," International Journal of Mechanical Science, **7**, pp. 531 – 538.

25. Hillier M.J., 1964, "The effect of pressure on the ductility of thin sheet subjected to some simple forming processes," The International Journal of Production Research, **3** (4), pp. 341 – 352.

26. Chakrabarty J., and Alexander J.M., 1969, "Plastic instability of thick-walled tubes with closed ends," International Journal of Mechanical Science, **1**, pp.175-186.

27. El-Sebaie M.G., and Mellor P.B., 1973, "Plastic instability conditions when deep-drawing into a high pressure medium," International Journal of Mechanical Science, **15**, pp. 485-501.

28. Carleer B., van der Kevie G., de Winter L., and van Veldhuizen B., 2000, " Analysis of the effect of material properties on the hydroforming process of tubes," Journal of Materials Processing Technology, **104**, pp. 158 – 166.

29. Manabe K., and Amino M., 2002, "Effects of process parameters and material properties on deformation process in tube hydroforming," Journal of Materials Processing Technology, **123**, pp. 285 – 291.

30. Bodeau N., Lejeune A., and Gelin J. C., 2002, "Influence of material and process parameters on the development and bursting in flange and tube hydroforming," Journal of Materials Processing Technology, **125 – 126**, pp. 849 – 855.

31. Koc M., 2003, "Investigation of the effect of loading path and variation in material properties on robustness of the tube hydroforming process," Journal of Materials Processing Technology, **133**, pp. 276 – 281.

32. Ahmed M., and Hashmi M.S.J., 1997, "Estimation of machine parameters for hydraulic bulge forming of tubular components," Journal of Materials Processing Technology, **64**, pp. 9-23.

33. Rimkus W., 1997, "Investigation into internal high pressure forming using finite element techniques," Transfer Report, University of Wolverhampton, Wolverhampton, United Kingdom.

34. Association of Engineers (VDI), 1999, Guideline VDI 3146, "Hydroforming –Basic Knowledge," Chapter 1 – Outline, pp1.

35. Asnafi N., and Skogsgardh A., 2000, "Theoretical and experimental analysis of stroke controlled tube hydroforming," Materials Science and Engineering, **A279**, pp. 95-110.

36. Rimkus W., Bauer H., and Mihsein M.J.A., 2000, "Design of load-curves for hydroforming applications," Journal of Materials Processing Technology, **108**, pp. 97-105.

37. T. Sokolowski, K. Gerke, M. KocË, M. Ahmetoglu, and T. Altan, 1998, "Evaluation of tube formability and material characteristics in tube hydroforming," ERC/NSM Report No. THF/ERC/NSM-98-R-025, Ohio State University, Columbus, OH.

38. Dohmann F., and Hartl C., 1996, "Hydroforming – a method to manufacture light weight parts," Journal of Materials Processing and Technology, 60, pp. 669-676.

39. Website of Variform (http://www.vari-form.com/index.shtml), "Automotive Applications," Variform, Warren, MI.

40. Longhouse B., 1999, "Automotive applications of hydroformed tubes," paper presented at the *SME Conference – Hydroforming Technologies,* March 10-11, Livonia, MI.

41. B. Viehweger, 1996, "With water to the shape" (in German), Blech Rohre Profile **43** (1-2), pp. 36-39.

42. Leitloff F.U., 1997, "Hydroforming - from feasibility analysis to series production," *Proceedings of the Second International Conference on Innovations in Hydroforming Technology*, Columbus, OH, September 17.

43. Birkert A., 1999, "Tool and part design for hydroforming," *Proceedings of the International Conference on Hydroforming*, Stuttgart, Germany, October 12-13.

44. Krei M., 1999, "State of the art of sealing for hydroforming," *Proceedings of the International Conference on Hydroforming*, Stuttgart, Germany, October 12-13.

45. Breckner M., 1999, "Hydraulic systems for hydroforming," *Proceedings of the International Conference on Hydroforming*, Stuttgart, Germany, October 12-13.

46. Klaas F., 1999, "Innovations in high pressure hydroforming," *Proceedings of the Second International Conference on Innovations in Hydroforming Technology*, Columbus, OH, September 17.

47. Ahmetoglu M., and Altan T., 2000, "Tube hydroforming: state-of-the-art and future trends," Journal of Materials Processing Technology, **98**, pp. 25 – 33.

48. Altan T., Koc M., Aue-u-lan Y., and Tiwari K., 1999, "Formability and design issues in tube hydroforming," *Proceedings of the International Conference on Hydroforming*, Fellbach-Suttgart, Germany, October 12-13.

49. Schmoeckel D., Hielscher C., Huber R., and Prier M., 1997, "Internal high pressure forming" (in German), PtU der Technischen Hochschule Darmstadt.

50. Prier M., and Schmoeckel D., 1999, "Tribology of internal pressure forming," *Proceedings of the International Conference on Hydroforming*, Stuttgart, Germany, October 12-13.

51. Dohmann F., Oct 1997 "Tribology in internal high pressure forming" (in German), Blech Rohre Profile pp. 36-39.

52. Vollertsen F., and Plancak M., 2002, "On possibilities for the determination of the coefficient of friction in hydroforming of tubes," Journal of Materials Processing Technology, **59** (39), pp. 1-9.

53. Pulzer J., 1998, "Fundamentals of tube bending," *Proceedings of the Workshop on Fundamentals of Hydroforming*, Nashville, TN, November 17.

54. Stange R., 1997, "Tooling and methods for tube and pipe bending," Tube and Pipe Journal, pp. 28 - 35.

55. Hutchinson M.I., 1988, "Bulge forming of tubular components," Ph.D. Thesis, Sheffield City Polytechnic, Sheffield, United Kingdom.

56. MacDonald B.J., and Hashmi M.S.J., 2000, "Finite element simulation of bulge forming of a cross-joint from tubular blank," Journal of Materials Processing Technology, **103**, pp. 333-342.

57. Duncan J. L., Hu J., and Marciniak Z., *Mechanics of Sheet Metal Forming*, Butterworth-Heinemann, Woburn, MA.

58. Asnafi N., 1999, "Analytical modeling of tube hydroforming," Thin-Walled Structures, **34**, pp. 295-330.

APPENDIX A

SIMULATION OF HYDROFORMING USING LS-DYNA

The Finite element simulation was carried out on LS-DYNA. The pre-processing was done on HYPERMESH. Post –processing was done on HYPERVIEW. The rigid tooling of tube hydroforming consists of (1) Die and (2) Axial punch. The entire pre-processing process can be divided into five steps:

1   Creating collectors

2   Creating geometry

3   Applying boundary condition

4   Updating cards

5   Control cards

A.1   Creating Collectors

Four types of collectors were created material (mat), property (prop), component (comp) and load collector.

A.1.1   Material Collector (*MAT)

Material Collector assigns the material properties to the part. Since dual hydroforming consists of total 3 parts (2 rigid parts and tube), 3 material collectors were created. All

the collectors are named according to the part. All the rigid toolings are specified *MAT_RIGID (MAT 20) which is the default rigid material for LS-DYNA. Tube was assigned *MAT_PIECEWISE_LINEAR_PLASTICITY (MAT24).

A.1.2   Property Collector (*SECTION_SHELL)

One shell section is created for die and punch and one for tube. Each section is assigned the corresponding part.

A.1.3   Component Collector (*PART)

Three component collectors were created and corresponding materials are assigned to each of them.

   a) Die – Rigid

   b) Punch – Rigid

   c) Tube – Piecewise linear plastic material

A.1.4 Load Collector (*BOUNDARY_PRESCRIBED_MOTION_RIGID)

A load collector for axial punch movement is created wherein displacement boundary condition in the *y* direction is prescribed.

A.2   **Creating Geometry**

Here a brief description is provided for modeling the parts of dual hydroforming process. Before starting to model any part, it is important to select the collector corresponding to the part to be modeled from the global menu. By this all the nodes and the elements that are created are assigned the property of that component.

A.2.1 Tube

Modeling of the tube was done using the user controlled cylinder. For this first the nodes were created for selecting the center of the die, major direction and normal direction. Radius, angle of the cylinder and the element density was used to complete the modeling.

A.2.2 Die

Modeling of the die was done using three user controlled cylinders and then trimming off the unnecessary geometry and filleting the corners.

A.2.3 Punch

Modeling of the punch was done using user controlled cylinder and combination of circle feature in geometry panel and spline function in 2d panel.

A.3 Boundary Condition

A.3.1 Contact

For defining the contact between different surface pair's two different types of contact algorithm were used.

A.3.1.1 CONTACT_SURFACE_TO_SURFACE_TITLE

This is used to define the surface contact between Tube- die and Tube – punch. Contact option is specified by selecting master surface and the slave surface. The rigid part was always selected as the master surface and the tube (which is finely meshed) was always selected as the slave surface.

The coefficient of static and dynamic friction between the Tube-die was specified as 0.10 and 0.00 respectively. The coefficient of static friction between the tube-punch was specified as 0.30.

A.3.1.2 CONTACT_SINGLE_SURFACE_TITLE

This is used to define contact for tube in the case of wrinkling. This contact definition would be used if tube surface comes in contact with itself, in case of wrinkling.

A.3.2 Pressure

An internal pressure of 40 MPa was applied to the tube. All the elements of the pressure component were selected. The magnitude and uniform size was specified. In a shell element pressure always acts in the direction of the normal so to reverse the direction of the pressure negative value of magnitude must be specified.

The external counter pressure was applied using LOAD_MASK option in LS-DYNA [29], which facilitates to apply a distributed load to a subset of elements of tube within a fixed global box.

A.3.3 Checking Penetration

Penetration option form the tools page was selected. Penetration check was done for a specified contact pair (interface). To avoid penetration two things have to be kept in mind, the normal of the contact pairs should be opposite to each other.If both the normal point towards each other then normal of one of the surface has to be reversed from the

normal menu on the tool's page. The slave surface (tube) should have a finer mesh than the master surface (rigid part). If there is a penetration then the element size of the tube needs to be decreased.

A.4 Updating Cards

This is the last step in creating the input deck.

A.4.1   Mat Collector

We have three materials made one for each part. Material property was specified by selecting the material collector. The property specified were: Young's modulus, density, poisons ratio. It is essential that units should be consistent because LS –DYNA does not have an inbuilt unit. The units selected here are:

Table A-1: Units used in Simulation

Mass	Ton
Force	N
Pressure	MPa
Time	sec
Displacement	mm

The other important thing which was specified is the translational and the rotational constraint of the rigid body.

A.4.1.1 Die

Die was constrained in all translational as well as rotational degree of freedoms.

A.4.1.2 Punch

Punch was constrained for x and z translation and rotations in all three axes. Only punch displacement in y direction was allowed.

A.4.1.3 Tube

Since only quarter model of the tube was discretized, it was necessary to constraint tube according to symmetric boundary conditions.

A.4.2 Property Collector

Shell element, thickness and NIP (number of integration points) was specified for each shell segment. Four noded, Belytschko- Tsay with 5 NIP having a thickness of 1.37 mm

was specified for the tube and Belytschko- Tsay with 2 NIP and thickness of 2.00 mm was specified for the rigid parts.

A.4.3 Component Collector

Material and section property is applied to the component (*PART) in this.

A.4.4 Load Collector

The translation of the punch was specified using *BOUNDARY_PRESCRIBED_MOTION_RIGID. Displacement boundary condition and load curve were defined. The load curve defines the displacement of the punch with respect to the time.

A.5   Control Cards

At the end control cards were added. By these cards the termination time, shell property, contact property and data base plots are defined.

APPENDIX B

INPUT DECK – DUAL HYDROFORMING

```
*KEYWORD
*TITLE
DUAL HYDROFORMING
$
$
$
$ Units: ton, mm, s, N, MPa, N-mm
$
$
$
$
$
*CONTROL_TERMINATION
$   endtim    endcyc     dtmin    endneg    endmas
  .100E-01         0      .000      .000      .000
$
*CONTROL_TIMESTEP
$   dtinit      scft      isdo    tslimt      dtms      lctm      erode ms1st
     .000      .400         0
$
*CONTROL_BULK_VISCOSITY
$       Q2        Q1
   1.500      .060
$
*CONTROL_CONTACT
$   slsfac    rwpnal    islchk    shlthk    penopt    thkchg     orien
     .100                             2
$   usrstr    usrfrc      nsbcs    interm     xpene     ssthk      ecdt    tiedpr
        0         0        10         0     4.000
$

$
*CONTROL_DAMPING
$   nrcyck     drtol     drfctr    drterm    tssfdr     irelal      edttl     idflg
      250      .001      .995
$
*CONTROL_ENERGY
$     hgen      rwen     slnten     rylen
        2         2         2         2
$
*CONTROL_HOURGLASS
$      ihq        qh
        1      .100
$
*CONTROL_OUTPUT
$    npopt    neecho     nrefup    iaccop     opifs    ipnint     ikedit
        1         3         0         0      .000         0       100
$
*CONTROL_SHELL
     20.0         1         0         1
$
*DATABASE_BINARY_D3PLOT
```

```
$        dt        lcdt
  .200E-03
$
*DATABASE_BINARY_D3THDT
$        dt        lcdt
  .000E+00
$
$
*DATABASE_EXTENT_BINARY
$    neiph     neips    maxint    strflg    sigflg    epsflg    rltflg    enflg
         0         0         3         1         1         1         1         1
$   cmpflg    ieverp    beamip
         0         0         0         0         0         0
$
*DATABASE_GLSTAT
$        dt
  .100E-03
$
$$$$$$$$$$$$$$$$$$$$$$$$$$$$$$$$$$$$$$$$$$$$$$$$$$$$$$$$$$$$$$$$$$$$$$$$$$$$$$$$$$$$
$
$
$$$$  Contacts
$
$$$$$$$$$$$$$$$$$$$$$$$$$$$$$$$$$$$$$$$$$$$$$$$$$$$$$$$$$$$$$$$$$$$$$$$$$$$$$$$$$$$$
$
$
$...>....1....>....2....>....3....>....4....>....5....>....6....>....7....>....
8
$
*CONTACT_SURFACE_TO_SURFACE_TITLE
$      cid       name
         3       IF1
$
$     ssid      msid     sstyp     mstyp    sboxid    mboxid       spr        mp
         3         2         3         3         0         0         0
0
$
$       fs        fd        dc        vc       vdc     penck        bt        dt
 0.300E+00 0.000E+00 0.000E+00 0.000E+00 0.000E+00         0 0.000E+00 1.00E+20
$
$      sfs       sfm       sst       mst      sfst      sfmt       fsf        vs
  .100E+01   .100E+01                      .098E+01   .098E+01   .100E+01   .10E+01
$
$
*CONTACT_SURFACE_TO_SURFACE_TITLE
$      cid       name
         4       IF4
$
$     ssid      msid     sstyp     mstyp    sboxid    mboxid       spr        mp
         3         1         3         3         0         0         0         0
$
$       fs        fd        dc        vc       vdc     pechk        bt        dt
 0.100E+00 0.000E+00 0.000E+00 0.000E+00 0.000E+00         0 0.000E+00 1.00E+20
$
$      sfs       sfm       sst       mst      sfst      sfmt       fsf        vf
  .100E+01   .100E+01                      .100E+01   .100E+01   .100E+01   .10E+01
$
$
*CONTACT_SINGLE_SURFACE_TITLE
$      cid       name
```

```
         5        IF5
$
$       ssid      msid     sstyp     mstyp     sbxid    mboxid       spr       mpr
         3         0         3         0         0         0         0         0
$
$        fs        fd        dc        vc       vdc     pechk        bt        dt
 0.000E+00 0.000E+00 0.000E+00 0.000E+00 0.000E+00         0 0.000E+00 1.00E+20
$
$       sfs       sfm       sst       mst      sfst      sfmt       fsf        vf
  .100E+01  .100E+01                           .100E+01  .100E+01  .100E+01  .10E+01
$
$$$$$$$$$$$$$$$$$$$$$$$$$$$$$$$$$$$$$$$$$$$$$$$$$$$$$$$$$$$$$$$$$$$$$$$$$$$$$$$$$$
$
$
$$$$   Parts and Materials
$
$$$$$$$$$$$$$$$$$$$$$$$$$$$$$$$$$$$$$$$$$$$$$$$$$$$$$$$$$$$$$$$$$$$$$$$$$$$$$$$$$$
$
$
$...>....1....>....2....>....3....>....4....>....5....>....6....>....7....>....
8
$
*PART
$       pid       sid       mid     eosid      hgid      grav    adpopt
die-1
         1         1         1
punch-2
         2         1         2
tube-3
         3         2         3
$
$$$$$  Materials
$
*MAT_RIGID
$       mid        ro         e        pr         n    couple         m      alas
         1 9.830E-09 2.070E+05 3.000E-01 0.000E+00 0.000E+00 0.000E+00
$       cmo      con1      con2
       1.0       7.0       7.0
$lco or a1        a2        a3        v1        v2        v3

$
*MAT_RIGID
$       mid        ro         e        pr         n    couple         m      alas
         2 9.830E-09 2.070E+05 3.000E-01 0.000E+00 0.000E+00 0.000E+00
$       cmo      con1      con2
       1.0       4.0       7.0
$lco or a1        a2        a3        v1        v2        v3

$
*MAT_PIECEWISE_LINEAR_PLASTICITY
$       mid        ro         e        pr      sigy      etan         R      HLID
         3 2.700E-09 0.700E+05 3.300E-01 5.000E+01 5.331E+02



$
$$$$$  Sections
$
*SECTION_SHELL
$       sid     elform      shrf       nip     propt    qr/irid     icomp
```

```
         1         2 .830E+00         2.0         1.0         .0
$        t1         t2         t3         t4       nloc
 2.000E+00 2.000E+00 2.000E+00 2.000E+00
$
*SECTION_SHELL
$       sid     elform       shrf        nip      propt    qr/irid      icomp
         2         2 .830E+00         5.0         1.0         .0
$        t1         t2         t3         t4       nloc
 1.370E+00 1.370E+00 1.370E+00 1.370E+00
$
$$$$$$$$$$$$$$$$$$$$$$$$$$$$$$$$$$$$$$$$$$$$$$$$$$$$$$$$$$$$$$$$$$$$$$$$$$$$$$$$$$
$
$
$$$$  Boundary Conditions
$
$$$$$$$$$$$$$$$$$$$$$$$$$$$$$$$$$$$$$$$$$$$$$$$$$$$$$$$$$$$$$$$$$$$$$$$$$$$$$$$$$$
$
$
$...>....1....>....2....>....3....>....4....>....5....>....6....>....7....>....
8
$
*BOUNDARY_PRESCRIBED_MOTION_RIGID
$       pid        dof        vad       lcid         sf        vid      death
         2         3         2         2      -12.0
$
*BOUNDARY_PRESCRIBED_MOTION_SET
$      nsid        dof        vad       lcid         sf        vid      death
         1         3         2         2      -12.0
$
*DEFINE_CURVE
$      lcid       sidr       scla       sclo       offa       offo
         1         0
$         abscissa           ordinate
     .000000000E+00     .000000000E+00
     .025000000E-01     .108000000E+01
     .100000000E-01     .137500000E+01
     .110000000E-01     .140000000E+01
$
*DEFINE_CURVE
$      lcid       sidr       scla       sclo       offa       offo
         2         0
$         abscissa           ordinate
     .000000000E+00     .000000000E+00
     .100000000E-01     .100000000E+01
     .110000000E-01     .110000000E+01
*DEFINE_BOX
         1  -36.0610    -1.0000    -0.9173    13.1500    -1.0000    12.1180
$
$
*DEFINE_VECTOR
         1  -11.2281     1.7785    10.7000   -36.0610     1.7785    10.7000
$
*DEFINE_CURVE
$      lcid       sidr       scla       sclo       offa       offo
         3         0                               7
$         abscissa           ordinate
     .000000000E+00     .000000000E+00
     .100000000E-01     .100000000E+01
$
$
```

```
*LOAD_MASK
         3         3         1         0         1         0
0
       300
$
*DEFINE_BOX
         2    1.0000   36.0610   -0.9173   13.1500   -1.0000   12.1180
$
$
*DEFINE_VECTOR
         2    9.0000    1.7785   10.7000   36.0610    1.7785   10.7000
$
*DEFINE_CURVE
$     lcid      sidr      scla      sclo      offa      offo
         4         0                   7
$       abscissa              ordinate
   .000000000E+00       .000000000E+00
   .100000000E-01       .100000000E+01
$
$
*LOAD_MASK
         3         4         2         0         2         0                   0
       300
$
*SET_NODE_LIST
$      sid
         1
$     nid1      nid2      nid3      nid4      nid5      nid6      nid7       nd8
      3061      3062      3093      3124      3155      3186      3217      3248
      3279      3310      3341      3372      3403      3434      3465      3496
      3527      3558      3589      3620      3651
$
*BOUNDARY_SPC_NODE
$      nid       cid      dofx      dofy      dofz     dofrx     dofry      dfrz
      3001         0         0         1         1         1         1         1
      3002         0         0         1         0         1         0         1
      3004         0         0         0         1         1         1         0
      3005         0         0         1         0         1         0         1
         ......
         ......
         ......
         ......
      3651         0         0         1         0         1         0         1
$
$$$$$$$$$$$$$$$$$$$$$$$$$$$$$$$$$$$$$$$$$$$$$$$$$$$$$$$$$$$$$$$$$$$$$$$$$$$$$$$$$$$
$
$
$$$$  Loading Conditions
$
$$$$$$$$$$$$$$$$$$$$$$$$$$$$$$$$$$$$$$$$$$$$$$$$$$$$$$$$$$$$$$$$$$$$$$$$$$$$$$$$$$$
$
$
$...>....1....>....2....>....3....>....4....>....5....>....6....>....7....>...8
$
*LOAD_SEGMENT
$     lcid        sf        at        n1        n2        n3        n4
         1    40.000                3001      3002      3003      3004
         1    40.000                3002      3005      3006      3003
         1    40.000                3005      3007      3008      3006
         1    40.000                3007      3009      3010      3008
```

```
          ......
          ......
          ......
          ......
$
$$$$$$$$$$$$$$$$$$$$$$$$$$$$$$$$$$$$$$$$$$$$$$$$$$$$$$$$$$$$$$$$$$$$$$$$$$$$$$$$$$$$$
$
$
$$$$  Define Nodes and Elements
$
$$$$$$$$$$$$$$$$$$$$$$$$$$$$$$$$$$$$$$$$$$$$$$$$$$$$$$$$$$$$$$$$$$$$$$$$$$$$$$$$$$$$$
$
$
$...>....1....>....2....>....3....>....4....>....5....>....6....>....7....>....
8
$
*NODE
$   nid              x              y              z    tc    rc
      500  11.59358672163 6.1987702467002 15.011666312014
      501 10.766142425477 7.5503753663949 13.868902609821
      502 9.8447191387781 8.7124433944825 12.596157300245
      503  8.859788261722 9.7123031230657 11.236004731365
      509 2.2893297191321 12.942773441101 2.1617229479731
      510 1.1461638781071 13.093661447114 0.5829361038426
        ......
        ......
        ......
        ......

     3651 -.113750000E+02  .442958800E-05  .534999900E+02
$
$$$$$$$$$     Shell Elements
$
*ELEMENT_SHELL
$   eid    pid     n1     n2     n3     n4
      500      1   1060   1161   1160   1160
      501      1    510    512    511    511
      502      1    547    546    548    548
      503      1    556    555    557    557
       .....
       ......
       ......
       ......

     2198      2   2227   2198   2209   2228
$
*END
```

APPENDIX C

STRESS AND STRAIN STATES

The stress and strain state at the mean diameter of the tube and thinning comparison between tube hydroforming and dual hydroforming shall be made at same bulge height. The comparison will be made for the condition that hoop strain is zero. The zero hoop strain implies there is no change in the mean diameter of the tube and the comparison will be made at this instantaneous point. Cylindrical co-ordinate system is chosen with r for radial direction, θ for hoop direction and z for axial direction (Fig. C-1).
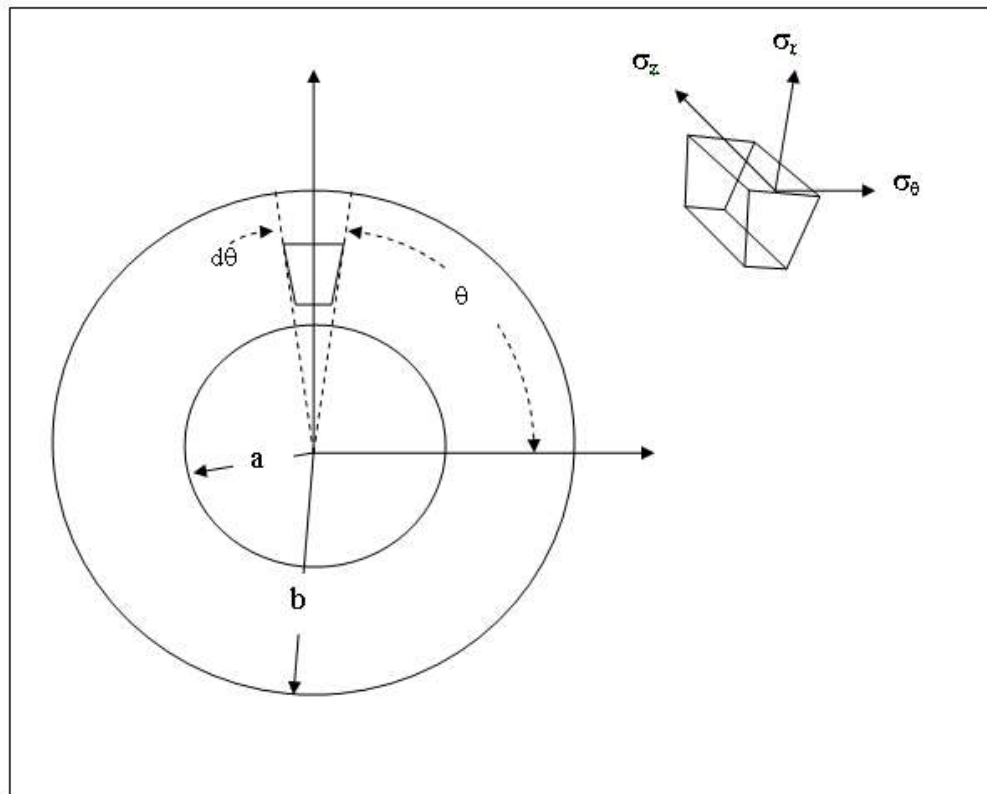
Figure C-1: Thin-walled Tube in Cylindrical Coordinates.

A straight tube is considered having internal radius '*a*' and outer radius '*b*'.

Let t_o be the initial thickness.

As reported by Ahmed et al. the punches enter a length of x_o at each end of the tube and the unconstrained length is x [32] (Fig. C-2).
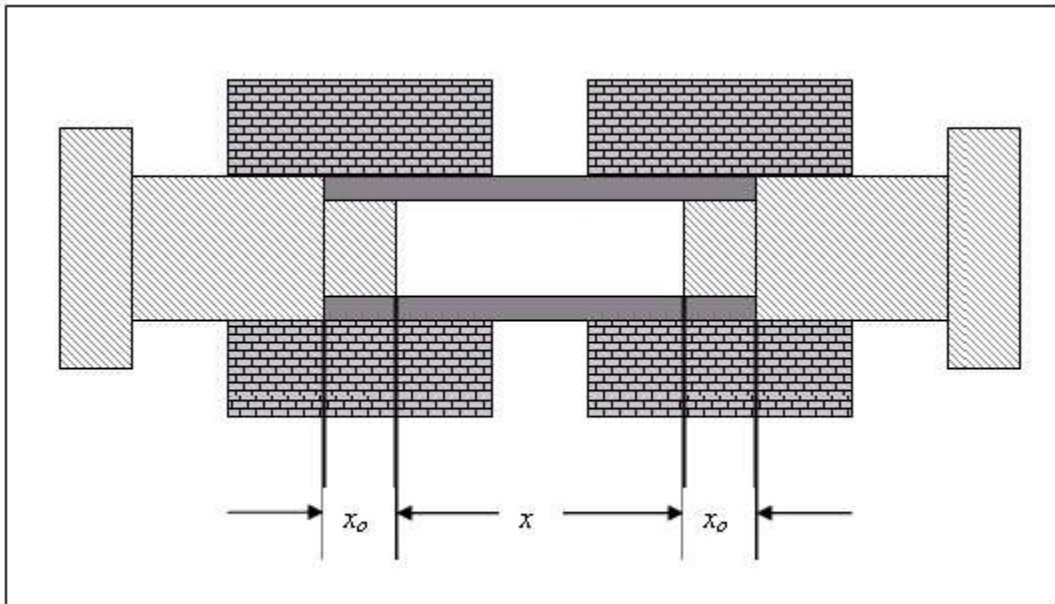

Figure C-2: Tube under Bulging

The analysis by Ahmed et al. was also based on the same assumption that the mean diameter of the tube will not change significantly i.e. zero strain in the hoop direction ($\varepsilon_\theta = 0$) [32].

Plane strain condition is considered wherein $\varepsilon_\theta = 0$, the volume constancy would give

$\varepsilon_t = -\varepsilon_z$. The deviatoric stress, $\sigma_\theta{}' = 0$.

The normal axial stress, $\sigma_\theta = \dfrac{1}{2}\left(\sigma_r + \sigma_z\right)$ (C-1)

Following vonMises Criterion,

$$\overline{\sigma} = \frac{1}{\sqrt{2}}\left[\left(\sigma_1 - \sigma_2\right)^2 + \left(\sigma_2 - \sigma_3\right)^2 + \left(\sigma_3 - \sigma_1\right)^2\right]^{1/2}$$ (C-2)

$$\sigma_1 = \sigma_r; \sigma_2 = \sigma_\theta; \sigma_3 = \sigma_z$$ (C-3)

Equation (C-3) in equation (C-2)

$$\overline{\sigma} = \frac{1}{\sqrt{2}}\left[\left(\sigma_r - \sigma_\theta\right)^2 + \left(\sigma_\theta - \sigma_z\right)^2 + \left(\sigma_z - \sigma_r\right)^2\right]^{1/2}$$ (C-4)

For the plane strain condition σ_θ is given by equation (C-1).

$$\overline{\sigma} = \frac{1}{\sqrt{2}}\left[\left(\sigma_r - \frac{1}{2}(\sigma_r + \sigma_z)\right)^2 + \left(\frac{1}{2}(\sigma_r + \sigma_z) - \sigma_z\right)^2 + \left(\sigma_r - \sigma_z\right)^2\right]^{1/2}$$ (C-5)

Simplifying equation (C-5)

$$\overline{\sigma} = \frac{\sqrt{3}}{2}\left(\sigma_r - \sigma_z\right)$$ (C-6)

$$\frac{2}{\sqrt{3}}\overline{\sigma} = \left(\sigma_r - \sigma_z\right)$$ (C-7)

At yielding, $\overline{\sigma} = \sigma_{yp}$,

$$\frac{2}{\sqrt{3}}\sigma_{yp} = \left(\sigma_r - \sigma_z\right)$$ (C-8)

From equation (C-1)

$$\sigma_r - \sigma_\theta = \frac{1}{2}(\sigma_r - \sigma_z) \qquad \text{(C-9)}$$

From equation (C-8) in equation (C-9),

$$\sigma_r - \sigma_\theta = \frac{\sigma_{yp}}{\sqrt{3}} \qquad \text{(C-10)}$$

For an element within the deformation zone the equilibrium of forces in the radial direction gives [32],

$$\frac{d\sigma_r}{dr} + \frac{\sigma_r - \sigma_\theta}{r} = \frac{-2mk}{x} \qquad \text{(C-11)}$$

where, m is the friction factor and k is the shear strength.

From equation (C-10) in equation (C-11)

$$\frac{d\sigma_r}{dr} + \frac{\sigma_{yp}}{\sqrt{3}r} = \frac{-2mk}{x} \qquad \text{(C-12)}$$

and for vonMises criterion, $\sigma_{yp} = \sqrt{3}k$ therefore,

$$\frac{d\sigma_r}{dr} + \frac{\sigma_{yp}}{\sqrt{3}r} = \frac{-2m\sigma_{yp}}{\sqrt{3}x} \qquad \text{(C-13)}$$

Rearranging equation (C-13)

$$d\sigma_r = -\frac{\sigma_{yp}}{\sqrt{3}r}dr - \frac{2m\sigma_{yp}}{\sqrt{3}x}dr \qquad \text{(C-14)}$$

which upon integration yields,

$$\sigma_r = -\frac{\sigma_{yp}}{\sqrt{3}r}\ln r - \frac{2m\sigma_{yp}}{\sqrt{3}x}r + C \qquad \text{(C-15)}$$

At $r = a$, $\sigma_{ra} = -p_i$, where $-p_i$ is the hydraulic pressure at the inner wall of the tube. Applying this boundary condition,

$$C = -p_i + \frac{\sigma_{yp}}{\sqrt{3}r}\ln a + \frac{2m\sigma_{yp}}{\sqrt{3}x}a \qquad \text{(C-16)}$$

therefore,

$$\sigma_r = -p_i - \frac{\sigma_{yp}}{\sqrt{3}r}\ln\frac{a}{r} - \frac{2m\sigma_{yp}(a-r)}{\sqrt{3}x} \qquad \text{(C-17)}$$

The axial stress at the inside surface of the deformation zone at radius $r = a$ is given by equation (C-8), whereby

$$\sigma_{za} = \sigma_{ra} - \frac{2}{\sqrt{3}}\sigma_{yp} = -p_i - \frac{2}{\sqrt{3}}\sigma_{yp} \qquad \text{(C-18)}$$

The radial stress at the outer surface of the tube within the deformation zone is σ_{rb} at $r = b$ from equation (C-17).

$$\sigma_{rb} = -p_i - \frac{\sigma_{yp}}{\sqrt{3}r}\ln\frac{a}{b} - \frac{2m\sigma_{yp}(a-b)}{\sqrt{3}x} \qquad \text{(C-19)}$$

Now if we consider external pressure p_o as shown in Fig. C-4, a simple force balance in radial direction would result in radial stress at $r = b$
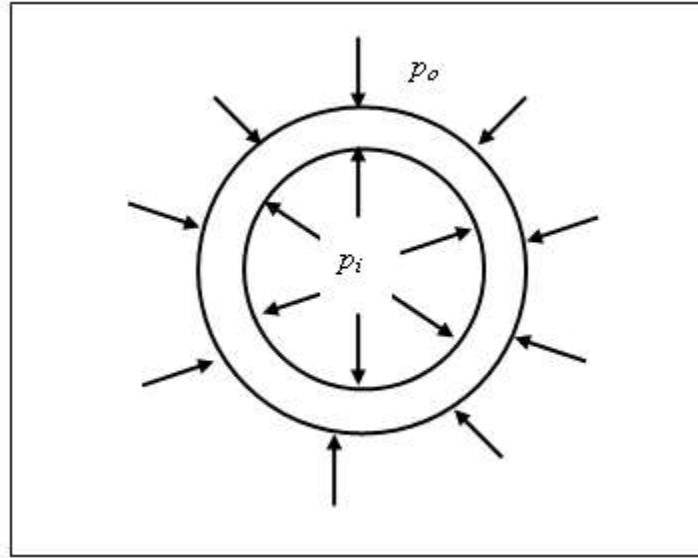
Figure C-3: Tube with Internal and External Pressure

Therefore from equation (C-19),

$$\sigma_{rb} = -p_i - \frac{\sigma_{yp}}{\sqrt{3}r}\ln\frac{a}{b} - \frac{2m\sigma_{yp}(a-b)}{\sqrt{3}x} - p_o \tag{C-20}$$

The axial stress at the outside surface of the deformation zone at radius $r = b$ is given by equation (C-8), whereby

$$\sigma_{zb} = \sigma_{rb} - \frac{2}{\sqrt{3}}\sigma_{yp} = -p_i - \frac{\sigma_{yp}}{\sqrt{3}r}\ln\frac{a}{b} - \frac{2m\sigma_{yp}(a-b)}{\sqrt{3}x} - p_o - \frac{2}{\sqrt{3}}\sigma_{yp} \tag{C-21}$$

APPENDIX D

PLASTIC INSTABILITY

D.1 Plastic Instability – Uniaxial Tensile Test

The stress σ_1 in the longitudinal direction is given by,

$$\sigma_1 = \frac{F}{A} \qquad \text{(D-1)}$$

where, F is the applied load over a cross-sectional area A.

Let a small additional longitudinal strain $\delta\varepsilon_1$ be imposed when the stress is σ_1.

From equation (D-1), work-hardening requires that the load F be increased by an amount

$$A\frac{d\sigma_1}{d\varepsilon_1}\delta\varepsilon_1 \qquad \text{(D-2)}$$

On the other hand, reduction of cross-sectional area corresponds to a reduction in load of

$$\sigma_1 \frac{dA}{d\varepsilon_1}\delta\varepsilon_1 \qquad \text{(D-3)}$$

An "incipient neck" is formed at some part of the bar [22]. The system is stable as long as the increase in load carrying capacity due to work hardening at any incipient neck can compensate for the decrease in load-carrying capacity due to reduction in cross-sectional area [22].

Therefore instability occurs when,

$$A\frac{d\sigma_1}{d\varepsilon_1}\delta\varepsilon_1 + \sigma_1\frac{dA}{d\varepsilon_1}\delta\varepsilon_1 = 0 \tag{D-4}$$

or

$$\frac{d\sigma_1}{\sigma_1} = -\frac{dA}{A} = -\frac{dl}{l} \tag{D-5}$$

$$\frac{d\sigma_1}{\sigma_1} = d\varepsilon_1 \tag{D-6}$$

Rearranging equation (D-6)

$$\frac{1}{\sigma_1}\frac{d\sigma_1}{d\varepsilon_1} = 1 \tag{D-7}$$

For uniaxial tensile test, $\overline{\sigma} = \sigma_1$ and $d\overline{\varepsilon} = d\varepsilon_1$ where, $\overline{\sigma}$ is the effective stress and $\overline{\varepsilon}$ is the effective strain.

Equation (D-7) changes to $\dfrac{1}{\overline{\sigma}}\dfrac{d\overline{\sigma}}{d\overline{\varepsilon}} = 1$ \hfill (D-8)

But $\dfrac{1}{\overline{\sigma}}\dfrac{d\overline{\sigma}}{d\overline{\varepsilon}} = \dfrac{1}{z}$ \hfill (D-9)

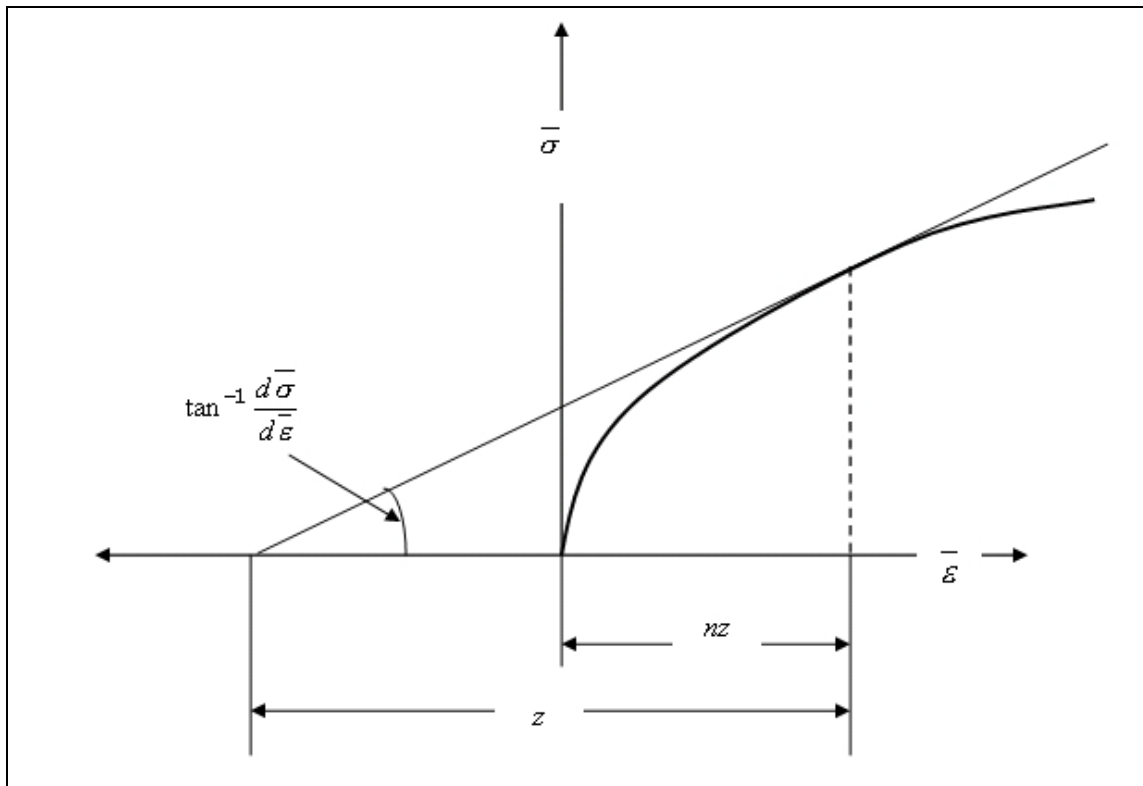where z is the sub-tangent modulus as shown in Fig D-1 and $\overline{\varepsilon} = nz$.

Figure D-1: Sub-tangent Modulus z

Therefore, the critical strain for the uniform tensile test from equation (D-8)

$$\bar{\varepsilon} = \varepsilon_1 = n(1) = n \qquad \text{(D-10)}$$

D.2 Plastic Instability - Thin Walled Tubes

As plastic instability criterion has to be established for dual hydroforming (additional counter pressure), a force balance analysis is done in the radial direction for the thin walled tubes (Fig. D-2). A section in cylindrical co-ordinate system is considered here where r is for radial, θ for hoop direction and z for axial direction.
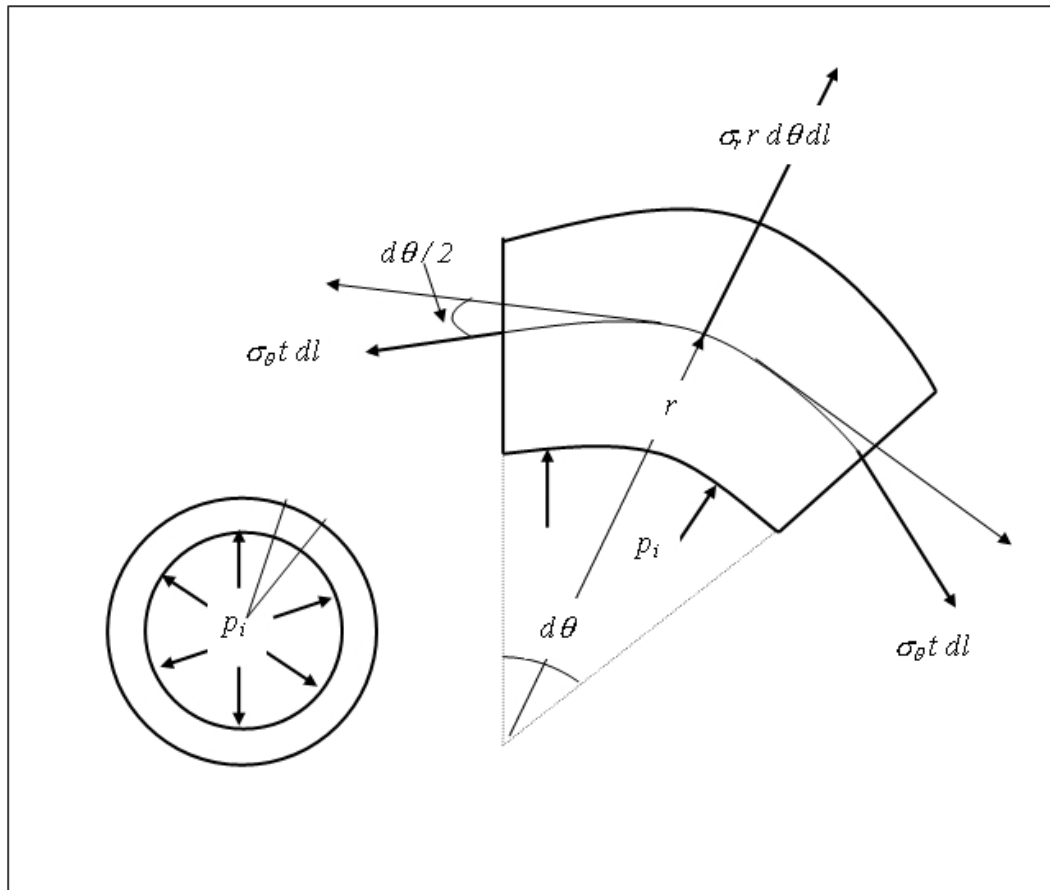
Figure D-2: Force Balance Analysis - Radial Direction

Balancing the forces along the radial direction from Fig. D-2,

$$p_i r d\theta dl + \sigma_r r d\theta dl = 2\sigma_\theta \sin\left(\frac{d\theta}{2}\right) t dl \qquad \text{(D-11)}$$

$$\sin\left(\frac{d\theta}{2}\right) \text{ is small} \approx \left(\frac{d\theta}{2}\right)$$

where, p_i is the internal pressure

　　　　r is the mean radius

dl is length of element in *z* direction

dθ is the small angle in hoop direction

Therefore, equation (D-11) becomes,

$$p_i r d\theta dl + \sigma_r r d\theta dl = 2\sigma_\theta \left(\frac{d\theta}{2}\right) t dl \tag{D-12}$$

$$p_i \frac{r}{t} + \sigma_r \frac{r}{t} = \sigma_\theta \tag{D-13}$$

The effective stress ($\overline{\sigma}$) given by vonMises Criterion,

$$\overline{\sigma} = \frac{1}{\sqrt{2}}\left[(\sigma_1 - \sigma_2)^2 + (\sigma_2 - \sigma_3)^2 + (\sigma_3 - \sigma_1)^2\right]^{1/2} \tag{D-14}$$

where σ_1, σ_2 and σ_3 are principal stresses.

The relation between effective stress, effective strain ($\overline{\varepsilon}$) and principal stresses using vonMises equation,

$$\frac{d\overline{\varepsilon}}{\overline{\sigma}} = \frac{d\varepsilon_1}{\sigma_1 - \frac{1}{2}(\sigma_2 + \sigma_3)} = \frac{d\varepsilon_2}{\sigma_2 - \frac{1}{2}(\sigma_3 + \sigma_1)} = \frac{d\varepsilon_3}{\sigma_3 - \frac{1}{2}(\sigma_1 + \sigma_2)} \tag{D-15}$$

For thin walled tube $\sigma_1 = \sigma_\theta; \sigma_2 = \sigma_z; \sigma_3 = \sigma_r$

D.2.2 Internal Pressure and Counter Pressure (DHF)

With internal pressure and external pressure of p_o,

$$\sigma_r \approx -p_o \qquad \text{(D-16)}$$

and, equation (D-13) becomes,

$$\sigma_\theta = (p_i - p_o)\frac{r}{t} \qquad \text{(D-17)}$$

A plane strain condition will be considered wherein $\varepsilon_z = 0$, the volume constancy would give $\varepsilon_t = -\varepsilon_\theta$. The deviatoric stress, $\sigma_z{}' = 0$.

The normal axial stress,

$$\sigma_z = \frac{1}{2}(\sigma_\theta + \sigma_r) \qquad \text{(D-18)}$$

The effective stress from equations (D-14) and (D-18)

$$\bar{\sigma} = \frac{1}{\sqrt{2}}\left[\left(\sigma_\theta - \frac{1}{2}(\sigma_\theta + \sigma_r)\right)^2 + \left(\frac{1}{2}(\sigma_\theta + \sigma_r) - \sigma_r\right)^2 + (\sigma_r - \sigma_\theta)^2\right]^{1/2} \qquad \text{(D-19)}$$

Simplifying equation (D-19),

$$\bar{\sigma} = \frac{\sqrt{3}}{2}(\sigma_\theta - \sigma_r) \qquad \text{(D-20)}$$

Rearranging equation (D-20),

$$\frac{2}{\sqrt{3}}\bar{\sigma} = (\sigma_\theta - \sigma_r) \qquad \text{(D-21)}$$

As, $\sigma_r \approx -p_o$

$$\frac{2}{\sqrt{3}}\overline{\sigma} = \left(\sigma_\theta + p_0\right) \tag{D-22}$$

$$\frac{2}{\sqrt{3}}\overline{\sigma} - p_0 = \sigma_\theta \tag{D-23}$$

Rearranging equation (D-17)

$$p_i = \sigma_\theta \frac{t}{r} + p_O \tag{D-24}$$

Let a small increment $\delta\overline{\varepsilon}$ be imposed when the stress is $\overline{\sigma}$.

From equation (D-24), work hardening requires that the internal pressure be increased by

an amount

$$\frac{t}{r}\frac{d\sigma_\theta}{d\overline{\varepsilon}}\delta\overline{\varepsilon} \tag{D-25}$$

From equation (D-23) in equation (D-25), work hardening requires that the internal

pressure be increased by an amount

$$\frac{t}{r}\frac{2}{\sqrt{3}}\frac{d\overline{\sigma}}{d\overline{\varepsilon}}\delta\overline{\varepsilon} \tag{D-26}$$

The change in geometry corresponds to a reduction in pressure of

$$\sigma_\theta \frac{d}{d\overline{\varepsilon}}\left(\frac{t}{r}\right)\delta\overline{\varepsilon} \tag{D-27}$$

From Equation (D-23) in equation (D-27), the change in geometry corresponds to a

reduction in pressure of

$$\left(\frac{2}{\sqrt{3}}\overline{\sigma} - p_o\right)\frac{d}{d\overline{\varepsilon}}\left(\frac{t}{r}\right)\delta\overline{\varepsilon} \tag{D-28}$$

Now,

$$\frac{d}{d\varepsilon}\left(\frac{t}{r}\right) = \frac{d}{dt}\frac{dt}{d\bar{\varepsilon}}\left(\frac{t}{r}\right) + \frac{d}{dr}\frac{dr}{d\bar{\varepsilon}}\left(\frac{t}{r}\right)$$
(D-29)

Using equation (D-18) in (D-15) we get,

$$\frac{d\bar{\varepsilon}}{\bar{\sigma}} = \frac{4}{3}\frac{d\varepsilon_\theta}{\left(\sigma_\theta - \sigma_r\right)} = -\frac{4}{3}\frac{d\varepsilon_t}{\left(\sigma_\theta - \sigma_r\right)}$$
(D-30)

As $\bar{\sigma} = \frac{\sqrt{3}}{2}\left(\sigma_\theta - \sigma_r\right)$ equation (D-30) reduces to,

$$d\bar{\varepsilon} = \frac{2}{\sqrt{3}}d\varepsilon_\theta = -\frac{2}{\sqrt{3}}d\varepsilon_t$$
(D-31)

$$d\varepsilon_\theta = \frac{dr}{r}$$
$$d\varepsilon_t = \frac{dt}{t}$$
(D-32)

From equations (D-31) and (D-32), we get

$$\frac{dr}{d\bar{\varepsilon}} = \frac{\sqrt{3}}{2}r$$
(D-33)

$$\frac{dt}{d\bar{\varepsilon}} = -\frac{\sqrt{3}}{2}t$$
(D-34)

Substituting equations (D-33) and (D-34) in equation (D-29), we get

$$\frac{d}{d\varepsilon}\left(\frac{t}{r}\right) = -\sqrt{3}\frac{t}{r}$$
(D-35)

Substituting equation (D-35) in equation (D-28), the change in geometry corresponds to

a reduction in pressure of

$$-\sqrt{3}\frac{t}{r}\left(\frac{2}{\sqrt{3}}\overline{\sigma}-p_o\right)\delta\overline{\varepsilon}$$ (D-36)

Using an argument of 'incipient bulging' similar to incipient necking in the simple tension test, the process will become unstable when the increase in internal pressure due to work hardening is balanced by the reduction in pressure due to geometry changes. That is, equation (D-26) + equation (D-36) = 0

$$\frac{t}{r}\frac{2}{\sqrt{3}}\frac{d\overline{\sigma}}{d\overline{\varepsilon}}\delta\overline{\varepsilon}+\left[-\sqrt{3}\frac{t}{r}\left(\frac{2}{\sqrt{3}}\overline{\sigma}-p_o\right)\delta\overline{\varepsilon}\right]=0$$ (D-37)

Dividing equation (D-37) by $\dfrac{2\overline{\sigma}}{\sqrt{3}}\dfrac{t}{r}$ and rearranging, we get

$$\frac{1}{\overline{\sigma}}\frac{d\overline{\sigma}}{d\overline{\varepsilon}}=\sqrt{3}\left(1-\frac{\sqrt{3}}{2}\frac{p_o}{\overline{\sigma}}\right)=\frac{1}{z}$$ where, z is the sub-tangent modulus (D-38)

Therefore, $$z=\frac{1}{\left(1-\sqrt{3}p_o\Big/2\overline{\sigma}\right)\sqrt{3}}$$ (D-39)

Hence, critical effective strain,

$$\overline{\varepsilon}^*=nz=\frac{n}{\left(1-\sqrt{3}p_o\Big/2\overline{\sigma}\right)\sqrt{3}}$$ (D-40)

D.2.2 Internal Pressure, Independent Axial Load and External Pressure (DHF)

With internal pressure and external pressure of p_o,

$$\sigma_r \approx -p_o \tag{D-41}$$

and, equation (D-13) becomes,

$$\sigma_\theta = (p_i - p_o)\frac{r}{t} \tag{D-42}$$

The analysis of the instability for a thin-walled tube under internal pressure, external pressure and independent axial loading, assumes the ratio of longitudinal to hoop stress remains constant and also the ratio of external pressure to hoop stress remains constant. This facilitates a simple theoretical analysis to bring out the difference in the plastic instability for varied boundary conditions.

Effective stress using equation (D-14),

$$\overline{\sigma} = \frac{1}{\sqrt{2}}\left[(\sigma_\theta - \sigma_z)^2 + (\sigma_z + p_o)^2 + (-p_o - \sigma_\theta)^2\right]^{\frac{1}{2}} \tag{D-43}$$

$$\overline{\sigma} = \frac{1}{\sqrt{2}}\left[\left(1 - \frac{\sigma_z}{\sigma_\theta}\right)^2 + \left(\frac{\sigma_z}{\sigma_\theta} + \frac{p_o}{\sigma_\theta}\right)^2 + \left(1 + \frac{p_o}{\sigma_\theta}\right)^2\right]^{\frac{1}{2}} \sigma_\theta \tag{D-44}$$

$$\overline{\sigma} = \lambda\sigma_\theta \tag{D-45}$$

where,

$$\lambda = \left[1 + \alpha^2 + \gamma^2 + \gamma\alpha - \alpha + \gamma\right]^{\frac{1}{2}} \tag{D-46}$$

and
$$\frac{p_o}{\sigma_\theta} = \gamma$$

$$\frac{\sigma_z}{\sigma_\theta} = \alpha$$

(D-47)

Rearranging equation (D-42), we get

$$\sigma_\theta \frac{t}{r} + p_o = p_i$$

(D-48)

In local bulging, let a small increment $\delta\bar{\varepsilon}$ be imposed when the stress is $\bar{\sigma}$.

From equation (D-48) work hardening requires that the internal pressure be increased by

an amount

$$\frac{t}{r} \frac{d\sigma_\theta}{d\bar{\varepsilon}} \delta\bar{\varepsilon}$$

(D-49)

From equation (D-45), in equation (D-49), work hardening requires that the internal

pressure be increased by an amount

$$\frac{t}{r} \frac{1}{\lambda} \frac{d\bar{\sigma}}{d\bar{\varepsilon}} \delta\bar{\varepsilon}$$

(D-50)

The change in geometry corresponds to a reduction in pressure of

$$\sigma_\theta \frac{d}{d\bar{\varepsilon}}\left(\frac{t}{r}\right)\delta\bar{\varepsilon}$$

(D-51)

From equation (D-45), in equation (D-51), the change in geometry corresponds to a

reduction in pressure of

$$\frac{\bar{\sigma}}{\lambda} \frac{d}{d\bar{\varepsilon}}\left(\frac{t}{r}\right)\delta\bar{\varepsilon}$$

(D-52)

Now,

$$\frac{d}{d\varepsilon}\left(\frac{t}{r}\right) = \frac{d}{dt}\frac{dt}{d\varepsilon}\left(\frac{t}{r}\right) + \frac{d}{dr}\frac{dr}{d\varepsilon}\left(\frac{t}{r}\right)$$
(D-53)

Using equations (15) and (D-53) we get,

$$\frac{d}{d\varepsilon}\left(\frac{t}{r}\right) = \frac{-3\sigma_\theta}{2\overline{\sigma}}\frac{t}{r}$$
(D-54)

Substituting equation (D-54) in (D-51), the change in geometry corresponds to a reduction in pressure of

$$\frac{-3\,\overline{\sigma}}{2}\frac{\sigma_\theta}{\lambda}\frac{t}{\overline{\sigma}}\frac{t}{r}\delta\overline{\varepsilon}$$
(D-55)

Using an argument of 'incipient bulging' similar to incipient necking in the simple tension test the process will become unstable when the increase in internal pressure due to work hardening is balanced by the reduction in pressure due to geometry changes.

That is, instability occurs when,

Equation (D-50) + Equation (D-55) = 0

$$\frac{t}{r}\frac{1}{\lambda}\frac{d\overline{\sigma}}{d\varepsilon}\delta\overline{\varepsilon} + \left[\frac{-3\,\overline{\sigma}}{2}\frac{\sigma_\theta}{\lambda}\frac{t}{\overline{\sigma}}\frac{t}{r}\delta\overline{\varepsilon}\right] = 0$$
(D-56)

Simplifying equation (D-56),

$$\frac{1}{\overline{\overline{\sigma}}}\frac{d\overline{\sigma}}{d\varepsilon} = \frac{3}{2}\frac{\sigma_\theta}{\overline{\sigma}}$$
(D-57)

From equation (D-45), $\bar{\sigma} = \lambda \sigma_\theta$, equation (D-57) changes to,

$$\frac{1}{\bar{\sigma}} \frac{d\bar{\sigma}}{d\bar{\varepsilon}} = \frac{3}{2} \frac{1}{\lambda} = \frac{1}{z} \quad \text{where, z is the sub-tangent modulus} \tag{D-58}$$

$$z = \frac{2}{3} \lambda = \frac{2}{3} \left[1 + \left(\frac{\sigma_z}{\sigma_\theta} \right)^2 + \left(\frac{p_o}{\sigma_\theta} \right)^2 + \left(\frac{\sigma_z}{\sigma_\theta} \frac{p_o}{\sigma_\theta} \right) - \left(\frac{\sigma_z}{\sigma_\theta} \right) + \frac{p_o}{\sigma_\theta} \right]^{\frac{1}{2}} \tag{D-59}$$

Hence, critical strain,

$$\bar{\varepsilon}^* = nz = \frac{2}{3} \left[1 + \left(\frac{\sigma_z}{\sigma_\theta} \right)^2 + \left(\frac{p_o}{\sigma_\theta} \right)^2 + \left(\frac{\sigma_z}{\sigma_\theta} \frac{p_o}{\sigma_\theta} \right) - \left(\frac{\sigma_z}{\sigma_\theta} \right) + \frac{p_o}{\sigma_\theta} \right]^{\frac{1}{2}} n \tag{D-60}$$

APPENDIX E

REDUCTION OF INSTABILITY CRITERION

The instability criterion for combined loading of internal pressure, axial load and counter pressure is given by

$$\bar{\varepsilon}^* = \frac{2}{3}\lambda n = \frac{2}{3}\left[1 + \left(\frac{\sigma_z}{\sigma_\theta}\right)^2 + \left(\frac{p_o}{\sigma_\theta}\right)^2 + \left(\frac{\sigma_z}{\sigma_\theta}\frac{p_o}{\sigma_\theta}\right) - \left(\frac{\sigma_z}{\sigma_\theta}\right) + \frac{p_o}{\sigma_\theta}\right]^{\frac{1}{2}} n \,.$$

Without axial load for $\sigma_z = \frac{1}{2}(\sigma_\theta + \sigma_r)$, the equation reduces to that thin tube subjected

to internal pressure and external pressure i.e. $\dfrac{n}{\left(1 - \sqrt{3}p_o \middle/ 2\bar{\sigma}\right)\sqrt{3}}$.

Effective stress using von Mises equation,

$$\bar{\sigma} = \frac{1}{\sqrt{2}}\left[(\sigma_1 - \sigma_2)^2 + (\sigma_2 - \sigma_3)^2 + (\sigma_3 - \sigma_1)^2\right]^{\frac{1}{2}} \tag{E-1}$$

As, $\sigma_z = \frac{1}{2}(\sigma_\theta + \sigma_r)$ equation (E-1) simplifies to

$$\bar{\sigma} = \frac{\sqrt{3}}{2}(\sigma_\theta - \sigma_r) \tag{E-2}$$

$$\bar{\sigma} = \frac{\sqrt{3}}{2}(\sigma_\theta + p_o) \tag{E-3}$$

$$\overline{\sigma} = \frac{\sqrt{3}}{2}\left(1 + \frac{p_o}{\sigma_\theta}\right)\sigma_\theta \tag{E-4}$$

Comparing with $\overline{\sigma} = \lambda\sigma_\theta$, we get

$$\lambda = \frac{\sqrt{3}}{2}\left(1 + \frac{p_o}{\sigma_\theta}\right) \tag{E-5}$$

The instability criterion for combined loading of internal pressure, axial load and counter pressure is given by,

$$\overline{\varepsilon}^* = \frac{2}{3}\lambda n \tag{E-6}$$

Putting value of (E-5) in (E-6), the plastic instability criterion becomes

$$\overline{\varepsilon}^* = \frac{2}{3}\frac{\sqrt{3}}{2}\left(1 + \frac{p_o}{\sigma_\theta}\right)n \tag{E-7}$$

$$\overline{\varepsilon}^* = \frac{1}{\sqrt{3}}\left(\frac{\sigma_\theta + p_o}{\sigma_\theta}\right)n \tag{E-8}$$

But, $\overline{\sigma} = \frac{\sqrt{3}}{2}(\sigma_\theta + p_o)$

Therefore, equation (E-8) reduces to

$$\overline{\varepsilon}^* = \frac{1}{\sqrt{3}}\left(\frac{\frac{2}{\sqrt{3}}\overline{\sigma}}{\frac{2}{\sqrt{3}}\overline{\sigma} - p_o}\right) \tag{E-9}$$

Dividing by $\frac{2}{\sqrt{3}}\overline{\sigma}$

$$\bar{\varepsilon}^* = \frac{n}{\left(1 - \sqrt{3}p_o \middle/ 2\bar{\sigma}\right)\sqrt{3}}$$ (E-10)

Equation (E-10) is the instability criterion for combined loading of internal pressure and counter pressure.

Hence, the instability criterion for combined loading of internal pressure, axial load and counter pressure reduces to that thin tube subjected to internal pressure and external pressure for $\sigma_z = \frac{1}{2}(\sigma_\theta + \sigma_r)$ i.e. no axial loading.

VITA

Nishant Jain

29 B 30 Gali No. 6, Friends Colony

G.T. Road, Shahadra, Delhi -110095, India

December 15, 1978..Born, Meerut, U.P., India

2001 – 2003...M.S. Mechanical Engineering,

Texas A&M University, USA

1996 - 2000..B.E. Mechanical Engineering,

Bangalore University, India

Email address: nishant_78@yahoo.com